Physical Review D LBL-38125RR

Statistical Properties of the Linear Sigma Model Used in Dynamical Simulations of DCC Formation*

Jørgen Randrup

Nuclear Science Division, Lawrence Berkeley National Laboratory
University of California, Berkeley, California 94720

November 1, 1996

Abstract:

The present work develops a simple approximate framework for initializing and interpreting dynamical simulations with the linear sigma model exploring the formation of disoriented chiral condensates in high-energy collisions. By enclosing the system in a rectangular box with periodic boundary conditions, it is possible to uniquely decompose the chiral field into its spatial average (the order parameter) and its fluctuations (the quasi-particles) which can be treated in the Hartree approximation. The quasi-particle modes are then described approximately by Klein-Gordon dispersion relations containing an effective mass depending on both the temperature and the magnitude of the order parameter; their fluctuations are instrumental in shaping the effective potential governing the order parameter; and the emerging statistical description is thermodynamicially consistent. The temperature dependence of the statistical distribution of the order parameter is discussed, as is the behavior of the associated effective masses; as the system is cooled the field fluctuations subside, causing a smooth change from the high-temperature phase in which chiral symmetry is approximately restored towards the normal phase. Of practical interest is the fact that the equilibrium field configurations can be sampled in a simple manner, thus providing a convenient means for specifying the initial conditions in dynamical simulations of the non-equilibrium relaxation of the chiral field; in particular, the correlation function is much more realistic than those emerging in previous initialization methods. It is illustrated how such samples remain approximately invariant under propagation by the unapproximated equation of motion over times that are long on the scale of interest, thereby suggesting that the treatment is sufficiently accurate to be of practical utility.

*This work was supported by the Director, Office of Energy Research, Office of High Energy and Nuclear Physics, Nuclear Physics Division of the U.S. Department of Energy under Contract No. DE-AC03-76SF00098, and by the National Institute for Nuclear Theory at the University of Washington in Seattle.

1 Introduction

The possibility of producing and observing disoriented chiral condensates in high-energy collisions of hadrons and nuclei has stimulated considerable interest over the past few years (for a recent review, see ref. [1, 2]). The basic premise is that the collision generates an extended domain of space within which chiral symmetry is approximately restored. If this happens, macroscopic pion fields may be generated as a consequence of the subsequent non-equilibrium relaxation towards the normal state. Such isospin-aligned domains may manifest themselves in anomalous pion emission [3, 4, 5] of the type seen in the Centauro cosmic ray events [6]. The experimental exploration of this phenomenon is of fundamental interest because it has a direct bearing on the mechanism of spontaneous chiral symmetry breaking. Efforts are well underway to search for the associated pion multiplicity fluctuations in proton-proton collisions [7].

In order to assess the prospects for such a phenomenon to actually occur and be detectable above the background of other pion production processes, it is necessary to perform extensive dynamical calculations. This is a daunting task because the chiral degrees of freedom should be properly embedded in the complicated environment generated in a high-energy collision which evolves from being primarily partonic at the early stage to entirely hadronic in the course of the chiral relaxation process. Fortunately, the study of suitable idealized scenarios can yield valuable insights regarding the prospects for observing the effect.

Most dynamical studies have been carried out within the framework of the linear σ model, treated in the mean-field approximation in which the chiral degrees of freedom are represented by a classical field [8, 9, 10, 11, 12, 13, 14, 15, 16, 17]. The present work seeks to provide a framework that may be useful for initializing and interpreting such calculations by elucidating how the commonly adopted simulation model behaves under the idealized conditions of statistical equilibrium, an aspect that has not yet been exhibited in the literature. A practical outcome of the work is the development of a simple and efficient approximate method for sampling field configurations from a given thermal ensemble. The motivations for undertaking the present work are primarily two-fold, as summarized below.

Since the linear σ model (in its relatively unsophisticated version employing classical fields) has been and still is the primary vehicle for simulating the dynamics of DCC formation, it is important to understand its actual properties. Having an insight into the statistical properties of the model makes it easier to interpret the dynamical behavior observed in the simulations. In particular, it provides a quantitative basis for assessing the degree of deviation from a mere adiabatic evolution, a key issue for DCC formation [18]. Moreover, knowing how the adopted simulation model behaves under equilibrium conditions makes it easier to assess its physical utility, since any inherent shortcomings of the model may all too easily be obscured by the complexities inherent in the dynamical evolution. Thus we are addressing the rather elementary issue of how the particular rather simplistic model in fact behaves in the context of numerical simulations, as opposed to issues concerning more refined versions of the model (such as those including quantum effects or partonic degrees of freedom). Indeed, the work should not be seen as an endorsement of that particular model as an accurate tool for DCC simulations but is merely intended to make judgments about its adequacy easier to make. (However, the method developed employed in our treatment is quite powerful and can be employed more generally, so in fact the work serves also as an instructive exposition of that method of analysis.)

An additional motivation for the present work concerns the manner of initialization of the chiral fields used in the simulations. The common method consists in setting up a spatial lattice and then simply picking the field strength at each site randomly from a suitable normal distribution. When one proceeds in this manner, the initial correlation function is ill-defined, since the field strengths at any two different lattice sites are uncorrelated. Effectively, one might say that the correlation length equals the lattice spacing, but such a dependence on a numerical parameter appears physically unacceptable. Moreover, that particular spatial dependence of the correlation function would hardly correspond to any physically plausible scenario. Although this kind of shortcoming might be less important in many cases, it should be a cause for concern in situations where instabilities are present, such as in the DCC context. Indeed, the observed pion spectrum is basically the Fourier transform of the correlation function and this quantity is, roughly speaking, merely a magnified/stretched version of the initial correlation function, especially in the hoped-for scenario of exponential amplification. It might therefore be useful to devise a physically better based method for initializing the field. Being able to sample configurations from a thermal ensemble of fields provides a conceptually simple way of characterizing the initialization. However, by developing a convenient approximate method for this task, we do not mean to suggest that the early dynamics in fact leads to a thermal form of the chiral field (the resolution of that issue must await specific guidance provided by partonic calculations) but merely to establish a much-improved method for initializing the dynamical simulations.

The scope of the present work is thus limited, as we are concerned primarily with problems that are relevant to the practical task of performing dynamical simulations with the linear σ model in the specific context of disoriented chiral condensates. Accordingly, it is not our intention to explore the entire space of model parameters but rather, we consider only one set parameter values close to those actually employed, which are adjusted to approximate the physical scenario encountered in nature where a small but finite symmetry-breaking term is present. In particular, the present work is not intended as a contribution towards the exploration of the $O(4)$-symmetric case which has already been studied extensively, albeit mostly from more formal perspectives [19, 20]. Indeed, while apparently quite a good approximation in the case of practical interest where a smooth cross over occurs as a function of temperature, the developed approximation may be inadequate in the symmetric scenario where a sharp phase transition is expected and, consequently, where even quantitatively small imperfections in the treatment may have a qualitative effect on the critical features.

After a brief reminder of the relevant features of the linear σ model (sect. 2), we describe how thermal equilibrium can be treated approximately by means of a standard linearization procedure invoking the Hartree approximation (sect. 3). We then discuss and illustrate the statistical distribution of the average field strength, the order parameter (sect. 4), and subsequently turn to the properties of the quasi-particle degrees of freedom associated with the spatial field fluctuations (sect. 5). An impression of the validity of the treatment is then gained by evolving samples of field configurations by the exact equation of motion (sect. 6). Finally, a concluding discussion is given (sect. 7).

2 The linear σ model

To set the framework for the subsequent developments, we start by briefly recalling the most relevant features of the formal framework. The present study is carried out within the mean-field approximation where the quantum field operators are replaced by their expectation values, thereby bringing the treatment to the level of classical field theory. This simplified treatment is expected to suffice for exploratory calculations. Naturally, the mean-field approximation is only a first step towards a more complete description.

The basic object of study is then the chiral field

$$\Phi(\boldsymbol{r},t)=\sigma(\boldsymbol{r},t)+i\boldsymbol{\tau}\cdot\boldsymbol{\pi}(\boldsymbol{r},t)\ , \tag{1}$$

where the three elements of the vector $\boldsymbol{\tau}$ are the Pauli matrices. Here the scalar field $\sigma(\boldsymbol{r},t)$ and the vector field $\boldsymbol{\pi}(\boldsymbol{r},t)$ are both real and can conveniently be combined into the $O(4)$ vector $\boldsymbol{\phi}=(\sigma,\boldsymbol{\pi})$.

In the linear σ model [22], one introduces a simple local effective interaction energy density,

$$V(\boldsymbol{\phi})=\frac{1}{\hbar^3c^3}\left[\frac{\lambda}{4}(\phi^2-v^2)^2-H\sigma\right]\ , \tag{2}$$

where ϕ denotes the magnitude of the $O(4)$ vector $\boldsymbol{\phi}$,

$$\phi^2\equiv\boldsymbol{\phi}\cdot\boldsymbol{\phi}=\sum_{j=0}^{3}\phi_j(\boldsymbol{r},t)^2=\sigma^2+\boldsymbol{\pi}\cdot\boldsymbol{\pi}\ , \tag{3}$$

with $j=0,1,2,3$ referring to the four chiral directions. The interaction V contains three parameters: λ, the strength of the symmetric term; v, the location of its minimum; and H, the strength of the symmetry-breaking term. As is commonly done, these parameters are fixed by specifying the pion decay constant, $f_\pi=92$ MeV, and the meson masses, $m_\pi=138\ \mathrm{MeV}/c^2$ and $m_\sigma=600\ \mathrm{MeV}/c^2$, leading to

$$\lambda\ =\ \frac{m_\sigma^2c^2-m_\pi^2c^2}{2f_\pi^2}=20.14\ , \tag{4}$$

$$v\ =\ \left[\frac{m_\sigma^2-3m_\pi^2}{m_\sigma^2-m_\pi^2}f_\pi^2\right]^{\frac{1}{2}}=86.71\ \mathrm{MeV}\ , \tag{5}$$

$$H\ =\ m_\pi^2c^2f_\pi=(120.55\ \mathrm{MeV})^3\ . \tag{6}$$

The precise values of the model parameters are immaterial, both in view of the simple nature of the model and, in particular, within the context of our present idealized study. The value for the hypothetical σ mass is the most commonly adopted one; for m_π we have used the weighted average of the three observed pion masses, and for the pion decay constant we have simply taken two thirds of the pion mass which gives a simple value within the range of experimental data (the current values being $f_{\pi^\pm} = 92.4 \pm 0.26$ MeV and $f_{\pi^0} = 84 \pm 3$ MeV [23]).

The lagrangian density is given by

$$\mathcal{L}(\boldsymbol{r},t) = \frac{1}{\hbar^3 c^3} \left[\frac{1}{2}(\hbar\partial_t \boldsymbol{\phi})^2 - \frac{1}{2}(\hbar c \nabla \boldsymbol{\phi})^2 - \frac{\lambda}{4}(\phi^2 - v^2)^2 + H\sigma \right] . \tag{7}$$

The corresponding energy density is then

$$\mathcal{H}(\boldsymbol{r},t) = \frac{1}{\hbar^3 c^3} \left[\frac{1}{2}\psi^2 + \frac{1}{2}(\hbar c \nabla \boldsymbol{\phi})^2 + \frac{\lambda}{4}(\phi^2 - v^2)^2 - H\sigma \right] , \tag{8}$$

where the time derivative $\boldsymbol{\psi} \equiv \hbar\partial_t \boldsymbol{\phi}$ is the canonical conjugate of the field strength.

The action generated by a given time evolution is given by $\mathcal{S} = \int d\boldsymbol{r}\, dt \mathcal{L}(\boldsymbol{r},t)$. By demanding that $\mathcal{S}$ be stationary with respect to arbitrary variations of both the field strength $\boldsymbol{\phi}(\boldsymbol{r},t)$ and its first derivatives, one obtains the associated equation of motion,

$$\Box\boldsymbol{\phi} + \lambda(\phi^2 - v^2)\boldsymbol{\phi} = H\hat{\boldsymbol{\sigma}} , \tag{9}$$

where $\Box = \hbar^2\partial_t^2 - \hbar^2 c^2 \triangle$ is the d'Alambert differential operator, and $\hat{\boldsymbol{\sigma}}$ denotes the unit vector in the σ direction. Since the equation of motion is of second order in time, the evolution of the system is fully determined once the initial values of the field strength $\boldsymbol{\phi}(\boldsymbol{r})$ and the associated time derivative $\boldsymbol{\psi}(\boldsymbol{r})$ have been specified.

3 Approximate treatment

We now discuss how the chiral system can be treated in a convenient approximate manner. For this purpose, we confine the system within a rectangular box and impose periodic boundary conditions.

3.1 Linearization

Our starting point is the equation of motion (9) for the field strength. It is natural to decompose the field,

$$\boldsymbol{\phi}(\boldsymbol{r},t) = \underline{\boldsymbol{\phi}}(t) + \delta\boldsymbol{\phi}(\boldsymbol{r},t) , \tag{10}$$

where the first term is the spatial average, $\underline{\boldsymbol{\phi}} \equiv <\boldsymbol{\phi}>$, so that $<\delta\boldsymbol{\phi}> = \mathbf{o}$. The average part of the field, $\underline{\boldsymbol{\phi}}$, is often referred to as the order parameter, whereas the spatial fluctuations, $\delta\boldsymbol{\phi}(\boldsymbol{r})$, may be considered as quasi-particle degrees of freedom representing elementary excitations relative to the constant field configuration [10]. The $O(4)$ direction of the order parameter plays a special role and it it convenient to employ a correspondingly aligned reference system, *i.e.* a system in which $\underline{\boldsymbol{\phi}} = (\phi_0, \mathbf{o})$ and $\delta\boldsymbol{\phi} = (\delta\phi_{||}, \delta\boldsymbol{\phi}_\perp)$. The thermal average $\prec \delta\boldsymbol{\phi}\, \delta\boldsymbol{\phi} \succ$ is then a diagonal 4×4 tensor, as can be demonstrated by elementary means.

Taking the spatial average of the full equation of motion (9) leads to an equation for time evolution of the order parameter $\underline{\phi}$ [24],

$$\hbar^2\partial_t^2\underline{\phi} + \lambda[\phi_0^2 + \prec \delta\phi^2 \succ + 2 \prec \delta\phi_{||}^2 \succ - v^2]\underline{\phi} = H\hat{\boldsymbol{\sigma}} \ , \tag{11}$$

In deriving this equation, we have replaced the spatial averages $< \cdot >$ by thermal averages $\prec \cdot \succ$, as may be justified for a system of dimensions larger than the correlation length (the fluctuations in different regions of the system are then independent and can therefore be assumed to reflect the thermal distribution from which the particular field was sampled). We shall use $\prec \delta\phi_\perp^2 \succ$ to denote the diagonal elements of the isotropic 3×3 tensor $< \delta\boldsymbol{\phi}_\perp \ \delta\boldsymbol{\phi}_\perp >$, so that $\prec \delta\phi^2 \succ = \prec \delta\phi_{||}^2 \succ + 3 \prec \delta\phi_\perp^2 \succ$ is the total fluctuation.[1] Furthermore, $< \delta\phi^2 \ \delta\boldsymbol{\phi} >$ vanishes by symmetry.

By subtracting the equation of motion for the order parameter, eq. (11), from the full equation of motion (9), it is possible to obtain approximate equations for the field fluctuations,

$$\left[\Box + \mu_{||}^2 c^4\right]\delta\phi_{||} \ = \ 0 \ , \tag{12}$$

$$\left[\Box + \mu_\perp^2 c^4\right]\delta\boldsymbol{\phi}_\perp \ = \ \mathbf{o} \ , \tag{13}$$

where the effective masses $\mu_{||}$ and $\mu_\perp$ are determined by the auxiliary gap equations,

$$\mu_{||}^2 c^4 \ \equiv \ \lambda\left(3\phi_0^2 + \prec \delta\phi^2 \succ + 2 \prec \delta\phi_{||}^2 \succ - v^2\right) \ , \tag{14}$$

$$\mu_\perp^2 c^4 \ \equiv \ \lambda\left(\phi_0^2 + \prec \delta\phi^2 \succ + 2 \prec \delta\phi_\perp^2 \succ - v^2\right) \ . \tag{15}$$

In arriving at this result, we have replaced products of two individual fluctuations by their respective thermal ensemble average values, $\delta\phi_j\delta\phi_{j'} \leadsto \prec \delta\phi_j\delta\phi_{j'} \succ$, and, furthermore, products containing three fluctuation factors have been contracted in the usual manner [15],

$$\delta\phi_j\delta\phi_{j'}\delta\phi_{j''} \leadsto \prec \delta\phi_j\delta\phi_{j'} \succ \delta\phi_{j''} + \prec \delta\phi_{j'}\delta\phi_{j''} \succ \delta\phi_j + \prec \delta\phi_{j''}\delta\phi_j \succ \delta\phi_{j'} \ . \tag{16}$$

Equations (12) and (13) describe the fluctuations as independent quasi-particles having the respective effective masses $\mu_{||}$ and $\mu_\perp$, which in turn are given in terms of the field fluctuations, eqs. (14) and (15). This self-consistent relationship can be stated explicitly by invoking the expression for the associated thermal equilibrium fluctuations,

$$\prec \delta\phi_{||}^2 \succ = \frac{\hbar^3 c^3}{\Omega}\sum_{\mathbf{k}}{}' \frac{1}{\epsilon_k}\frac{1}{\mathrm{e}^{\epsilon_k/T} - 1} \ \asymp \ \frac{T}{2\pi^2}\ \mu_{||}c^2 \sum_{n>0}\frac{1}{n}K_1\left(n\frac{\mu_{||}c^2}{T}\right) \ , \tag{17}$$

and similarly for $\prec \delta\phi_\perp^2 \succ$. The system is enclosed in a rectangular box with the volume $\Omega = L_x L_y L_z$ and periodic boundary conditions are imposed. The wave vectors $\mathbf{k}$ are then quantized ($k_x L_x = 2\pi K_x$ with $K_x = 0, \pm 1, \ldots$, *etc.*), so that the

[1] We call attention to the fact that in the present notation $\prec \delta\phi_\perp^2 \succ$ denotes the variance of the field fluctuations in one of the transverse directions, whereas in refs. [10, 14] it represents three times that amount, namely the sum of the variances in all three perpendicular directions.

individual quasi-particle modes are enumerated by (K_x, K_y, K_z). The corresponding quasi-particle energy is determined by the dispersion relation $\epsilon_k^2 = \hbar^2 c^2 k^2 + \mu^2 c^4$, where the effective masses $\mu_{||}$ and $\mu_\perp$ lead to the energies $\epsilon_k^{||}$ and $\epsilon_k^\perp$, respectively. Finally, the prime on the summation sign indicates that the mode having $k = 0$ should be omitted since it represents the order parameter rather than a spatial fluctuation.

In eq. (17), the symbol $\asymp$ indicates the thermodynamic limit $L \to \infty$ in which the quasi-particle modes form a continuum. The fluctuations can then be expressed analytically in terms of the Modified Bessel Function K_1, as indicated. Generally, the fluctuations decrease as the effective mass increases, for a fixed temperature T, and $\prec \delta\phi_j^2 \succ = T^2/12$ when the effective mass μ_j vanishes. The global approximation $\prec \delta\phi_j^2 \succ \approx (T^2/12)(1 + \mu c^2/2\pi T)\exp(-\mu c^2/T)$ is good to better than 2%.

The treatment above has been carried out under the simplifying assumption of thermal equilibrium which suffices for our present purposes. However, it is interesting to note that the results can be readily generalized to non-equilibrium scenarios by simply replacing the thermal averages $\prec \cdot \succ$ by the corresponding spatial averages $< \cdot >$. In this manner, the system of equations would be closed and a conceptually simple dynamical description emerges. However, since the direct interaction between the quasi-particles is then ignored, any relaxation can occur only via the mean field, and the accuracy of such an approach should therefore be carefully assessed.

3.2 Effective masses

Utilizing the result (17), the coupled equations (14–15) for the effective masses can be solved for specified values of the temperature T and the magnitude ϕ_0, provided that these parameters are sufficiently large, and we then have $\mu_{||} \geq \mu_\perp \geq 0$. It should be noted that the effective masses are independent of the parameter H, since the symmetry-breaking term $H\sigma$ is linear.[2]

In fig. 1 we show the resulting effective masses $\mu_{||}$ and $\mu_\perp$ as functions of ϕ_0, for temperatures T up to well above critical. At any temperature, there is always a physical solution to the coupled equations (14-15) for the effective masses when $\phi_0 \geq v$. This is easy to see from eq. (15): At $T = 0$, when the fluctuations vanish, we have $\mu_\perp^2 = \lambda(\phi_0^2 - v^2)$ and so $\mu_\perp^2$ vanishes at $\phi_0 = v$ and is positive for larger ϕ_0; an increase of T will always increase the fluctuations, and hence the mass. Moreover, we always have $\mu_{||} \geq \mu_\perp$.

Since the field fluctuations and the magnitude of the order parameter contribute to the effective masses in qualitatively similar ways, an increase of the temperature (and thus the fluctuations) will permit a further decrease of ϕ_0, so that the point at which $\mu_\perp$ vanishes is moved to ever smaller values of ϕ_0. The appearance of $\mu_{||}$, considered as a function of ϕ_0, is nearly independent of temperature, except that each curve terminates at the point where the corresponding $\mu_\perp$ vanishes. This limiting curve is

[2]This simplifying feature holds only when λ, v, and H are considered as the primary model parameters. When H vanishes it is often customary to readjust the other two parameters, $\lambda = m_\sigma^2 c^2/2f_\pi^2 = 21.27$ and $v = f_\pi = 92$ MeV, and then the effective masses change correspondingly.

indicated by the dotted curve on the interval $(0, v)$ and it is elementary to calculate,

$$\phi_0^2 = v^2 - \frac{5}{12}T^2 - \prec \delta\phi_{\parallel}^2 \succ \approx v^2 - \frac{T^2}{12}(5 + \mathrm{e}^{-\mu_{\parallel}c^2/T}) , \quad (18)$$

$$\mu_{\parallel}^2 c^4 = \lambda(2v^2 - T^2) . \quad (19)$$

This behavior continues until the temperature reaches the value T_0, the lowest temperature for which there is a solution to eqs. (14-15) for all values of ϕ_0. For this particular temperature both effective masses vanish for $\phi_0 = 0$. Consequently, $\prec \delta\phi_j^2 \succ = T_0^2/12$ and so $T_0^2 = 2v^2$, *i.e.* $T_0 = 122.63$ MeV with the adopted parameter values.[3] The degeneracy in the masses, $\mu_{\parallel} = \mu_{\perp}$, is a general consequence of the $O(4)$ rotational symmetry that emerges for $\phi_0 = 0$ and it therefore remains as T is further increased, with the common mass value μ_0 increasing steadily. Since the effective mass at $\phi_0 = 0$ is given by $\mu_0^2 c^4 = \lambda(6 \prec \delta\phi_j^2 \succ - v^2)$, it becomes proportional to T at high temperatures, $\mu_0 c^2 \approx 1.59\ T$ for $T \gg v$.

The results displayed in fig. 1 have been calculated in the thermodynamic limit, $L \to \infty$, in which the quasi-particle modes form a continuum. However, the systems of interest in connection with high-energy nuclear collisions have finite volumes. The quasi-particle energies are then discrete and, as a result, the effective masses are modified. This effect is largest when the effective mass is small, *i.e.* near the critical conditions, because the absence of the constant mode in (17) is then most significant, and it generally leads to smaller masses. Figure 2 shows the temperature dependence of the effective masses for either $\phi_0 = 0$ or for $\phi_0 = f_\pi$ (the value associated with the physical vacuum), as obtained either in the continuum limit or for a cubic box with a side length L of either 8 fm or 5 fm.

For $\phi_0 \approx 0$ and temperatures near critical, the effective masses are significantly reduced. As a consequence, the associated critical temperature is increased to 154 MeV for $L = 8$ fm and to 172 MeV for $L = 5$ fm. However, for temperatures several tens of MeV above these thresholds, the effect is relatively small. The effect also disappears quickly as the order parameter is moved away from zero and by the time it reaches its vacuum value, $\phi_{\mathrm{vac}} = f_\pi = 92$ MeV, there is hardly any effect for even the smallest box ($L = 5$ fm).

The effect of the finite size on the fluctuations in the field strength is illustrated in fig. 3. The upper curves show the typical magnitude of the thermal fluctuations, $(\prec \delta\phi^2 \succ)^{1/2}$, as functions of ϕ_0 over a range of temperatures, for the same three box sizes as in fig. 2, while the lower curves show the continuum result for the contribution arising from fluctuations directed along the order parameter $\underline{\phi}$, $\prec \delta\phi_{\parallel}^2 \succ^{1/2}$. The fluctuations are remarkably independent of the volume, except in the critical region $T \approx T_0$ and $\phi_0 \approx 0$, as just discussed. For $\phi_0 = 0$ the $O(4)$ symmetry implies that the fluctuations are the same in all directions so that each of the lower curves starts out at half the value of the corresponding upper curve. For larger values of ϕ_0 the relative

[3]The special temperature T_0 is here used to denote that unique value of T for which the effective masses are when the order parameter vanishes. It is occasionally referred to as the "critical temperature" and denoted T_c but we find this nomenclature unfortunate, since the transition from approximate chiral symmetry to a broken phase generally occurs at significantly higher temperatures, as we shall illustrate later on.

contribution from fluctuations along $\underline{\phi}$ decreases progressively, since $\mu_{\|}$ grows much larger than $\mu_{\perp}$ (see fig. 1).

3.3 Energy

It is instructive to examine the total energy of the system. It is obtained by integrating the energy density (8) over the volume of the box,

$$\begin{aligned}\mathcal{E}(t) &= \int d\boldsymbol{r}\ \mathcal{H}(\boldsymbol{r},t) \ = \ \Omega < \frac{1}{2}\hbar^2\psi^2 + \frac{1}{2}\hbar^2c^2(\nabla\boldsymbol{\phi})^2 + V > &(20)\\ &= \Omega(E_0 + E_{\rm qp} + \delta V)\ . &(21)\end{aligned}$$

The total energy is conserved in time when the field is evolved with the equation of motion (9). The energy is composed of the three basic contributions exhibited in the second expression: one arising from the time dependence of the field strength, another associated with the spatial variation of the field, and a third resulting from the interaction. In the last expression, these contributions have been reorganized into three different terms which we will now discuss in turn.

The first term is the bare energy density, *i.e.* the energy density that would arise if the field had no spatial variation, $\boldsymbol{\phi} = \underline{\boldsymbol{\phi}}$ and $\boldsymbol{\psi} = \underline{\boldsymbol{\psi}}$,

$$E_0 = \frac{1}{\hbar^3c^3}\left[\frac{1}{2}\psi_0^2 + \frac{\lambda}{4}(\phi_0^2 - v^2)^2 - H\phi_0\cos\chi_0\right] = K_0 + V_0\ . \tag{22}$$

We have here introduced χ_0 to denote the angle of disorientation, *i.e.* the angle between the four-dimensional order parameter $\underline{\boldsymbol{\phi}}$ and the σ direction. The spatial average of σ is then $\sigma_0 = \underline{\boldsymbol{\phi}}\cdot\hat{\boldsymbol{\sigma}} = \phi_0\cos\chi_0$, and the corresponding mean magnitude of the pion field is $\pi_0 = \phi_0\sin\chi_0$. In the last expression K_0 denotes the kinetic part of E_0 and V_0 is the bare potential energy density.

The second term in (21) denotes the energy density associated with the quasi-particle degrees of freedom, in the approximation that these form a gas of independent particles,

$$\begin{aligned}E_{\rm qp} &= \frac{1}{\hbar^3c^3}\sum_{j=0}^{4}\frac{1}{2} < (\hbar\partial_t\delta\phi_j)^2 + (\hbar c\nabla\delta\phi_j)^2 + \mu_j^2c^4\delta\phi_j^2 > &(23)\\ &= \frac{1}{\hbar^3c^3}\sum_{j=0}^{4}\frac{1}{2}{\sum_{\mathbf{k}}}'(|\psi_{\mathbf{k}}^{(j)}|^2 + (\hbar^2k^2c^2 + \mu_j^2c^4)|\phi_{\mathbf{k}}^{(j)}|^2)\ . &(24)\end{aligned}$$

We have here invoked the general Fourier expansions of $\boldsymbol{\phi}(\boldsymbol{r})$ and $\boldsymbol{\psi}(\boldsymbol{r})$,

$$\begin{aligned}\boldsymbol{\phi}(\boldsymbol{r},t) &= \sum_{\mathbf{k}}\boldsymbol{\phi}_{\mathbf{k}}(t)\ \mathrm{e}^{i\mathbf{k}\cdot\boldsymbol{r}}\ , &(25)\\ \boldsymbol{\psi}(\boldsymbol{r},t) &= \sum_{\mathbf{k}}\boldsymbol{\psi}_{\mathbf{k}}(t)\ \mathrm{e}^{i\mathbf{k}\cdot\boldsymbol{r}}\ . &(26)\end{aligned}$$

The expansion coefficients are generally complex and are given simply in terms of spatial averages, $\boldsymbol{\phi}_{\mathbf{k}} =< \boldsymbol{\phi}(\boldsymbol{r})\exp(-i\mathbf{k}\cdot\boldsymbol{r}) >$ and $\boldsymbol{\psi}_{\mathbf{k}} =< \boldsymbol{\psi}(\boldsymbol{r})\exp(-i\mathbf{k}\cdot\boldsymbol{r}) >$. We note that the components with $\mathbf{k}=\mathbf{o}$ represent the order parameter, $\boldsymbol{\phi}_{\mathbf{O}}=\underline{\boldsymbol{\phi}}$ and $\boldsymbol{\psi}_{\mathbf{O}}=\underline{\boldsymbol{\psi}}$. Furthermore, the fact that the chiral field is real imposes the relations $\boldsymbol{\phi}_{\mathbf{k}}^{*}=\boldsymbol{\phi}_{-\mathbf{k}}$ and $\boldsymbol{\psi}_{\mathbf{k}}^{*}=\boldsymbol{\psi}_{-\mathbf{k}}$.

The third term in (21) corrects for the fact that the quasi-particles in fact interact via the fourth-order term in V,

$$\delta V \;=\; \frac{\lambda}{4}[<\delta\phi^4> \;-2<\delta\phi^2>^2 \;-4\sum_{j=0}^{3}<\delta\phi_j^2>^2] \;\approx\; -\frac{\lambda}{4}<\delta\phi^4> \;. \qquad (27)$$

The last result can be obtained by using the Gaussian approximation to express $<\delta\phi^4>$ in terms of squares of quadratic terms.

The energy of the system can be calculated as a function of the order parameter, assuming that the quasi-particle degrees of freedom are in thermal equilibrium. The resulting energy density is

$$E(\underline{\boldsymbol{\psi}},\underline{\boldsymbol{\phi}})=E_0(\psi_0,\phi_0,\chi_0)+\;\prec E_{\rm qp}\succ(\phi_0)+\;\prec\delta V\succ(\phi_0)=K_0+V_T(\phi_0,\chi_0)\;, \qquad (28)$$

where we have exhibited the dependence of the individual terms on the various parts of the order parameter. Here the thermal equilibrium value of the quasi-particle energy density is given by

$$\prec E_{\rm qp}^{(j)}\succ\;=\;\frac{1}{\Omega}{\sum_{\mathbf{k}}}'\frac{\epsilon_k}{{\rm e}^{\epsilon_k/T}-1}\;\asymp\;\frac{(\mu c^2)^4}{\hbar^3c^3}\frac{1}{2\pi^2}\sum_{n>0}\left[3\frac{\tau^2}{n^2}K_2(\frac{n}{\tau})+\frac{\tau}{n}K_1(\frac{n}{\tau})\right] \qquad (29)$$

for each of the four chiral directions j, with $\tau\equiv T/\mu_jc^2$. It can be expressed analytically in the continuum limit, as indicated. Furthermore, the thermal equilibrium value of the correction term is quite well represented by its Gaussian approximation,

$$\prec\delta V\succ\approx\;-\frac{\lambda}{4}[\prec\delta\phi^2\succ^2\;+2\prec\delta\phi_{\|}^2\succ^2\;+6\prec\delta\phi_{\perp}^2\succ^2]\;. \qquad (30)$$

In the last expression in (28) the energy has been split into the kinetic energy associated with the time dependence of the order parameter, $K_0=\psi_0^2/2\hbar^3c^3$, and the remainder which can be regarded as an effective potential for the order parameter,

$$V_T(\phi_0,\chi_0)\;=\;V_0+\;\prec E_{\rm qp}\succ\;+\;\prec\delta V\succ\;. \qquad (31)$$

This effective potential has been plotted in fig. 4 for the particular situation when the order parameter $\underline{\boldsymbol{\phi}}$ is directed along the σ axis, for a range of temperatures T. The directional dependence of V_T is simply given by the term $H\phi_0\cos\chi_0/\hbar^3c^3$. At zero temperature the effective potential can only be displayed for order parameters whose magnitude ϕ_0 exceed v, since only then can the effective masses be calculated, as explained in sect. 3.2: For smaller values of ϕ_0 some of the low-energy quasi-particle modes are unstable and so have no well-defined thermal equilibrium. As the temperature is increased, the domain of stability extends ever lower towards $\phi_0=0$. The limiting curve connecting the end points of all the subcritical curves is determined by the condition that $\mu_\perp$ vanish, implying $\mu_{\|}^2=\lambda(2v^2-T^2)$. The result is shown on the figure as the dotted curve between $\phi_0=0$ and $\phi_0=v$.

If H were zero the effective potential would have $O(4)$ symmetry and its minima would then form a degenerate surface of a 4-sphere. The presence of the linear symmetry-breaking term, $-H\sigma$, tilts the potential towards the σ direction and, consequently, there is only one minimum for any given temperature and it is located on the positive part of the σ axis. The minima of the effective potential move gradually towards larger values of the order parameter as the temperature is increased. In this respect, the results are similar to the behavior of the energy of nuclear matter as a function of the density ρ (see, for example, ref. [25]). However, while the energetics alone thus favors ever larger values of either ϕ_0 or ρ as the temperature is raised, the proper incorporation of the phase space (by means of the appropriate entropy) turns the picture around, as we shall now see.

4 The order parameter

We can now consider the distribution of the chiral field in statistical equilibrium at a given temperature T. Since the equation of motion (9) is of second order in time, we need to specify both the field strength $\boldsymbol{\phi}(\boldsymbol{r})$ and its time derivative $\boldsymbol{\psi}(\boldsymbol{r}) \equiv \hbar\partial_t\boldsymbol{\phi}(\boldsymbol{r})$ in order to fully characterize a state. As we have already exploited above, the quasi-particle degrees of freedom can be regarded as a Bose-Einstein gas having thermal distributions determined by their respective effective masses, in the appropriate domain of ϕ_0. Their behavior can then be calculated once the order parameter has been specified.

4.1 The partition function

It is natural to start the discussion of statistical properties by considering the partition function for the chiral field. It is obtained by summing the canonical weights for all the possible states,

$$\mathcal{Z}_T \equiv \int \mathcal{D}[\boldsymbol{\psi},\boldsymbol{\phi}]\ \mathrm{e}^{-\mathcal{E}[\boldsymbol{\psi},\boldsymbol{\phi}]/T} = \prod_{\mathbf{k}} \left[\int d^4\boldsymbol{\psi}_{\mathbf{k}}\ d^4\boldsymbol{\phi}_{\mathbf{k}}\right] \mathrm{e}^{-\frac{\Omega}{T}(E_0+\delta V+E_{\mathrm{qp}})} \tag{32}$$

$$\approx \int d^4\underline{\boldsymbol{\psi}}\ d^4\underline{\boldsymbol{\phi}}\ \mathrm{e}^{-\frac{\Omega}{T}(E_0+\prec\delta V\succ)}\mathcal{Z}_{\mathrm{qp}} = \int d^4\underline{\boldsymbol{\psi}}\ d^4\underline{\boldsymbol{\phi}}\ W_T(\underline{\boldsymbol{\phi}},\underline{\boldsymbol{\psi}})\ , \tag{33}$$

where $\mathcal{E}$ is the total energy of the system given in eqs. (20-21). The functional integral over all states $(\boldsymbol{\psi}(\boldsymbol{r}),\boldsymbol{\phi}(\boldsymbol{r}))$ has first been expressed as a multiple integral over the four-dimensional Fourier amplitudes $\boldsymbol{\psi}_{\mathbf{k}}$ and $\boldsymbol{\phi}_{\mathbf{k}}$ (see eqs. (25-26)). If the integration over the field fluctuations (*i.e.* those amplitudes having $\mathbf{k} \neq \mathbf{o}$) is performed, the remaining integrand is the statistical weight W_T expressing the relative probability for finding the system with a specified value of the order parameter. In order to derive an expression for W_T, we have replaced the state-dependent correction term δV (eq. (27)) by its approximate thermal average $\prec \delta V \succ$ (eq. (30)), for each value $(\underline{\boldsymbol{\psi}},\underline{\boldsymbol{\phi}})$ of the order parameter (it depends only on ϕ_0). The integral over the quasi-particle degrees of freedom can then be performed and yields the quasi-particle partition function $\mathcal{Z}_{\mathrm{qp}}$ (which also depends only on ϕ_0).

This quantity factorizes into contributions from each of the four chiral directions, $\mathcal{Z}_{\rm qp} = \prod_j \mathcal{Z}_{\rm qp}^{(j)}$, where

$$\mathcal{Z}_{\rm qp}^{(j)} \equiv \prod_{\mathbf{k}}{}' \left[\int d\psi_{\mathbf{k}}^{(j)}\, d\phi_{\mathbf{k}}^{(j)}\right] \mathrm{e}^{-E_{\rm qp}^{(j)}/T} \sim \prod_{\mathbf{k}}{}' \left[\int_0^\infty \epsilon_k dC_{\mathbf{k}}^2 \int_0^{2\pi} d\eta_{\mathbf{k}}\right] \mathrm{e}^{-E_{\rm qp}^{(j)}/T} . \tag{34}$$

Since the complex Fourier amplitudes $\psi_{\mathbf{k}}^{(j)}$ and $\phi_{\mathbf{k}}^{(j)}$ are subject to symmetry relations under $\mathbf{k} \to -\mathbf{k}$, as already noted above, is it more convenient to use the representation in terms of trigonometric functions, eqs. (46) and (48). The different wave numbers are then fully decoupled, and for each $\mathbf{k}$ the integration variables are the (positive) amplitude $C_{\mathbf{k}}$ and the associated phase $\eta_{\mathbf{k}}$, as indicated in the last expression above. The phases are unimportant here since they each merely contribute a factor of 2π. Moreover, the combination $n_{\mathbf{k}} \equiv \epsilon_k C_{\mathbf{k}}^2/\hbar^3 c^3$ can be interpreted as the average number of quanta in the mode $\mathbf{k}$ (see eq. (47)). Since we want to take account of the quantal nature of the quasi-particle degrees of freedom (see 5.1.1), we replace the continuous integral over $n_{\mathbf{k}}$ by a discrete sum over the possible integer values of the occupation number, thereby obtaining the standard expression for an ideal Bose-Einstein gas,

$$\mathcal{Z}_{\rm qp}^{(j)} \sim \prod_{\mathbf{k}}{}' \left[\sum_{n_{\mathbf{k}}=0}^{\infty} \mathrm{e}^{-n_{\mathbf{k}}\epsilon_k/T}\right] = \prod_{\mathbf{k}}{}'(1-\mathrm{e}^{-\epsilon_k/T})^{-1} = \prod_{\mathbf{k}}{}' \bar{f}_k^{(j)} . \tag{35}$$

We have used the fact that the quasi-particle energy is additive, $E_{\rm qp}^{(j)} = \sum_{\mathbf{k}} n_{\mathbf{k}}\epsilon_k$. Furthermore, $\bar{f}_k \equiv 1 + f_k$ where $f_k = (\mathrm{e}^{\epsilon_k/T} - 1)^{-1} = \prec n_{\mathbf{k}} \succ$ is the mean number of quanta (in the chiral direction j) having a wave number of magnitude k, and the corresponding energy ϵ_k is determined by $\epsilon_k^2 = \hbar^2 c^2 k^2 + \mu_j^2 c^4$.

It follows that the free energy density of the quasi-particles is $F_{\rm qp} = \sum_j F_{\rm qp}^{(j)}$ with

$$F_{\rm qp}^{(j)} \equiv -\frac{T}{\Omega} \ln \mathcal{Z}_{\rm qp}^{(j)} = \frac{1}{\Omega}\sum_{\mathbf{k}}{}' \left[\epsilon_k f_k - T(\bar{f}_k \ln \bar{f}_k - f_k \ln f_k)\right] = \prec E_{\rm qp}^{(j)} \succ - T S_T^{(j)} . \tag{36}$$

In the resulting expression, $\prec E_{\rm qp}^{(j)} \succ$ is the average thermal energy density of the quasi-particle modes associated with the chiral direction j, eq. (29), and $S_T^{(j)}$ is their entropy density. The total entropy density at the temperature T is then $S_T = S_T^{\|} + 3S_T^{\perp}$, where $S_T^{\|}(\phi_0)$ represents the entropy density of the field fluctuations along the direction of $\underline{\phi}$ [26],

$$S_T^{\|} = \frac{1}{\Omega}\sum_{\mathbf{k}}{}' \left[\bar{f}_k^{\|} \ln \bar{f}_k^{\|} - f_k^{\|} \ln f_k^{\|}\right] \tag{37}$$

$$\asymp \frac{1}{\hbar^3 c^3} \int_{\mu_\| c^2}^{\infty} \frac{d\epsilon}{2\pi^2}\, \epsilon\, (\epsilon^2 - \mu_\|^2 c^4)^{\frac{1}{2}} \left[\bar{f}(\epsilon) \ln \bar{f}(\epsilon) - f(\epsilon) \ln f(\epsilon)\right] . \tag{38}$$

and the contribution to the entropy density from fluctuations in a perpendicular direction, $S_T^{\perp}(\phi_0)$, can be calculated analogously by replacing $\mu_\|$ with $\mu_\perp$.

It is evident from the display of the effective potential, fig. 4, that the energetics alone would favor rather large magnitudes of the order parameter. However, the entropy of quasi-particles is higher at small values of ϕ_0, since the effective masses are then smaller, for a given temperature.[4] This interplay between energy and phase-space is conveniently quantified in the statistical weight (see eq. (33)),

$$W_T(\underline{\psi},\underline{\phi}) \equiv \int \mathcal{D}[\psi',\phi'] \, \mathrm{e}^{-\mathcal{E}[\psi',\phi']/T} \, \delta^4(\underline{\psi}'-\underline{\psi}) \, \delta^4(\underline{\phi}'-\underline{\phi}) \tag{39}$$

$$\approx \mathrm{e}^{-\frac{\Omega}{T}(K_0+V_0+\prec\delta V\succ+F_{\mathrm{qp}})} = \mathrm{e}^{-\frac{\Omega}{T}(K_0+F_T)} \tag{40}$$

We have used the decomposition (21) of the total energy and replaced δV by its thermal average $\prec \delta V \succ$ which causes the partition function to factorize. In the last expression, we have introduced the free energy density for the order parameter, $F_T(\underline{\phi}) = V_T(\phi_0, \chi_0) - T S_T(\phi_0)$.

The free energy density is illustrated in fig. 5 for a range of temperatures above which the trend is obvious. Since the entropy density of a free gas at fixed T goes up when the particle mass is reduced, the entropy provides a restoring force towards symmetry (recall that a reduction of the order parameter ϕ_0 leads to smaller effective masses). As a result, for increasing temperatures the minimum of the free energy density approaches $\phi_0 = 0$, but since H is finite it always remains on the positive part of the σ axis. As the temperature is reduced, the minimum in F_T moves smoothly outwards, with the most rapid change occurring near $T \approx 220$ MeV. The resulting behavior is shown by the solid curve in fig. 6 which will be discussed below.

4.2 Contact with other approaches

The present semiclassical treatment of the linear σ model is both conceptually and practically simple, but its quantitative utility of course depends on how well it emulates the properties obtained with more refined treatments.

Within the narrow context of the present study, namely the preparation of chiral field configurations for use in dynamical simulations of *DCC* formation, the most relevant reference treatments would be those invoking more standard renormalization schemes in conjunction with Hartree factorization techniques [11, 15]. However, for practical reasons, these quantal approaches retain only the leading order in a $1/N$ expansion and so it is less straightforward to assess the accuracy of the particular manner in which divergencies are avoided in the present approach. The situation is well illustrated by the behavior of the critical boundary, the curve along which the effective pion mass vanishes, $\mu_\perp = 0$. This curve starts at $\phi_0 = v$ at zero temperature. In the treatments of refs. [11, 15] the curve attains the value $\phi_0 = 0$ at the $T_0 = \sqrt{3}v$. If a similar $1/N$ truncation were made in the present treatment, the identical value would be obtained. However, our treatment makes no $1/N$ expansion and instead yields $T_0 = \sqrt{2}v$. It is interesting to compare this value with the result obtained by Tetradis and Wetterin who have made a more general investigation of the temperature dependent effective potential in ϕ^4 theories with a new method based on average fields [20]. For the dimensionality of interest, $N = 4$, their numerically determined critical

[4] The importance of the quasi-particle entropy in determining the statistical properties of the model was already emphasized by Bardeen and Moshe [27] a decade ago.

temperature is $T_0 \approx \sqrt{2.05}v$ which is in very good quantitative agreement with the result of the present treatment.

With regard to the behavior of the equilibrium value of the order parameter ϕ_0 (the solid curve displayed in fig. 6), recent preliminary and unpublished results obtained with the quantum density matrix approach [28] display a qualitatively similar behavior, although the decrease of ϕ_0 as the system is heated proceeds at a somewhat slower pace (*i.e.* the cross over from the broken to the restored phase is gentler). While the rough agreement between the two types of calculation suggests that the present implicit renormalization scheme is reasonable, detailed quantitative comparisons with the methods of refs. [11, 15] would be less informative at this point because of the significant effect of their $1/N$ truncation.

Furthermore, as will be discussed in sect. 4.3.2, the temperature at which the σ mass exhibits its minimum ($T_\chi \approx 240$ MeV) is in good accordance with an estimate ($T_\chi \approx 226$ MeV) made by Pisarski based on a gauged linear sigma model [29].

Finally we note that the present approach and those of refs. [11, 15] all invoke a Hartree factorization and it would therefore be interesting to undertake a study of how important this key approximation is. This issue remains open for future study.

4.3 Distributions

The preceding analysis implies that the statistical weight $W_T(\underline{\psi}, \underline{\phi})$, which is defined on the eight-dimensional phase space of the order parameter, in fact depends on only three quantities: the speed $\psi_0 = |\underline{\psi}|$, the magnitude $\phi_0 = |\underline{\phi}|$, and the disalignment angle χ_0. Moreover, since the entropy depends only on the effective masses, which in turn are determined solely by ϕ_0, the dependence of the free energy on the direction of $\underline{\phi}$ arises only through the symmetry-breaking H term in the interaction V (eq. (2)). Consequently, the corresponding projected probability distribution factorizes,

$$\begin{aligned} P_T(\psi_0, \phi_0, \chi_0) \;&\equiv\; \int d^4\underline{\psi}' \int d^4\underline{\phi}'\ \delta(\psi_0' - \psi_0)\ \delta(\phi_0' - \phi_0)\ \delta(\chi_0' - \chi_0)\ W_T(\underline{\psi}', \underline{\phi}') \\ &=\; P_\psi(\psi_0)\ P_\phi(\phi_0)\ P_\chi(\phi_0; \chi_0)\ \sim\ \psi_0^3\ \phi_0^3\ \sin^2\chi_0\ W_T(\psi_0, \phi_0, \chi_0)\ . \end{aligned} \tag{41}$$

Here ψ_0^3 and ϕ_0^3 are the Jacobians associated with the transformation from the four-dimensional vectors $\underline{\psi}$ and $\underline{\phi}$ to their magnitudes ψ_0 and ϕ_0, respectively, and $\sin^2\chi_0$ is the Jacobian arising from the three-dimensional nature of the space perpendicular to the order parameter $\underline{\phi}$. Furthermore, the three normalized probability densities are given by

$$P_\psi(\psi_0) \;=\; \mathcal{N}_\psi\ \psi_0^3\ \exp[-\frac{\Omega}{\hbar^3 c^3}\frac{\psi_0^2}{2T}]\ , \tag{42}$$

$$P_\phi(\phi_0) \;=\; \mathcal{N}_\phi\ \phi_0^3\ \exp[-\Omega(\frac{1}{T}V_T(\phi_0, \chi_0 = 0) - S_T(\phi_0))]\ , \tag{43}$$

$$P_\chi(\phi_0; \chi_0) \;=\; \mathcal{N}_\chi(\phi_0)\ \sin^2\chi_0\ \exp[-\frac{\Omega}{\hbar^3 c^3}\frac{H}{T}\phi_0(1 - \cos\chi_0)]\ . \tag{44}$$

For the normalization constants we have $\mathcal{N}_\psi^{-1} = 2\kappa^2$, with the convenient abbreviation $\kappa \equiv T\hbar^3 c^3/\Omega$, and $\mathcal{N}_\chi^{-1} = (\pi/\xi) I_1(\xi) \exp(-\xi)$, with $\xi \equiv H\phi_0/\kappa$.

The kinetic part, $P_\psi(\psi_0)$, is the projection of an isotropic four-dimensional normal distribution having a total variance of $\prec \psi_0^2 \succ = 4\kappa$. The average kinetic energy associated with the time evolution of the order parameter is then $\prec K \succ = 4T$, as would be expected in four dimensions. The mean speed is $\prec \psi_0 \succ = \sqrt{9\pi\kappa/8}$.

Considered as a function of the four-dimensional order parameter $\underline{\phi}$, the probability density has a maximum where the free energy has a minimum, as is evident from eq. (39). However, the jacobian factor $\sim \phi_0^3$ associated with the projection from $\underline{\phi}$ to ϕ_0 increases the most probable value of the magnitude ϕ_0. This effect depends on volume Ω, as is illustrated in fig. 6. The results for a finite box with $L = 8$ fm (dashed curve) are nearly identical to those obtained for $L \to \infty$, while $L = 5$ fm (dots) leads to a more significant increases in ϕ_0 at the higher temperatures. The most rapid increase of ϕ_0 occurs near $T \approx 200$ MeV which is well above the critical temperature T_0 (arrow) at which the effective masses drop to zero. We finally note that for relatively low temperatures the Jacobian causes the most probable value of ϕ_0 to slightly exceed the vacuum value.

The directional distribution $P_\chi(\phi_0; \chi_0)$, which depends parametrically on the magnitude ϕ_0, grows broader at high temperature where ϕ_0 decreases. In the temperature range considered here, up to several hundred MeV, $P_\chi(\chi_0)$ is well approximated by the projection of a three-dimensional normal distribution with a total variance of $3/\xi$, and the average magnitude of the disalignment angle χ_0 is then $\prec \chi_0 \succ \approx \sqrt{8/\pi\xi}$.

It is interesting to note that although the free energy associated with the special case of $H = 0$ has a qualitatively different appearance, displaying an $O(4)$-symmetric surface of degenerate minima, the corresponding curve for the most probable ϕ_0 largely exhibits the same behavior as observed for the finite value of H when finite volumes of nuclear size are considered, as illustrated in fig. 6 by the open dots. This remarkable feature is due to the statistical fluctuations which, when combined with the bias due to the jacobian factor ϕ_0^3 (see eq. (43)), cause the behavior of $P(\phi_0)$ to become relatively insensitive to the value of H. Of course, as the box size is increased, $L \to \infty$, the fluctuations will subside and $P(\phi_0)$ will become narrowly peaked around the lowest minimum of the free energy. This somewhat academic case is discussed further in sect. 6.3.

4.3.1 Distribution of the order parameter

For any finite volume Ω, the order parameter exhibits fluctuations around its most probable value. The full width at half maximum of the ϕ_0 distribution is shown by the horizontal bars in fig. 6 for the smallest box ($L = 5$ fm) where the fluctuations are the largest. The relative smallness of the fluctuations indicates that the order parameter is distributed within a rather limited range of values. This feature is further illustrated in fig. 7 which depicts the entire distribution, $P_\phi(\phi_0)$, over a range of temperatures, for a cubic box with side length $L = 8$ fm, which is our standard scenario. The solid curves in fig. 7 have been obtained by scaling the continuum results to the finite volume. The dashed curves show the effect of properly quantizing the problem (*i.e.* summing over the discrete modes rather than integrating). The effect is very small, because the distributions are peaked well inside the respective domains of stability.

For small temperatures, the distribution is narrowly peaked near the vacuum value $\phi_{\rm vac}{=}f_\pi$ (indicated by the arrow). As the temperature is increased, the distribution broadens and gradually begins to move inwards towards smaller values of ϕ_0. The width of the distribution increases from zero at $T = 0$, exhibits a maximum near $T \approx 220$ MeV, and then slowly shrinks as $T \to \infty$. The somewhat counterintuitive decrease of the fluctuations at high temperatures is due to by the fact that the growing thermal fluctuations cause the interaction to become progressively more repulsive, causing the effective potential V_T to become ever more confining.

We recall that for low temperatures, $T < T_0$, our treatment can only be carried out above a temperature-dependent minimum value of ϕ_0. As it turns it, this principal limitation is of little practical import. For example, for $T = 80$ MeV (the lowest temperature shown in fig. 7) the distance from the centroid (at ≈ 91 MeV) to the boundary (at ≈ 69 MeV) is over ten times the dispersion of the distribution (≈ 2 MeV). Thus, for any temperature, the distribution $P_\phi(\phi_0)$ is sufficiently narrow to make incursions into the respective unstable regime extremely unlikely.

A more global impression of the statistical distribution of the order parameter $\underline{\phi}$ can be obtained by considering a contour diagram of the projected probability density $P(\phi_0, \chi_0) \equiv P_\phi(\phi_0)\ P_\chi(\phi_0; \chi_0)$. Such a plot is displayed in fig. 8 for a box with $L = 8$ fm. The abscissa is the projection of the order parameter onto the σ axis, $\sigma_0 \equiv \underline{\phi} \cdot \hat{\sigma} = \phi_0 \cos\chi_0$, and the ordinate is the magnitude of its perpendicular component, $\pi_0 \equiv \phi_0 \sin\chi_0$. For each temperature, the dots show the location of the maximum and the half-maximum contours are traced out. The solid contours and dots refer to the continuum treatment, whereas the dashed contours and the open dots (shown for two temperatures only) are obtained with a quantized treatment, which is seen to have little effect. The profiles in fig. 7 are the projections of $P(\phi_0, \chi_0)$ onto the magnitude ϕ_0. It is evident from the above results that the $O(4)$ symmetry is far from restored at the temperatures expected in the planned high-energy nuclear collisions. Instead the order parameter is in fact distributed within a fairly limited domain around the σ axis, with both its magnitude ϕ_0 and its angle of disalignment χ_0 exploring only rather narrow ranges.

4.3.2 Distribution of the effective masses

The effective masses are functions of the magnitude of the order parameter, $\mu_{||}(\phi_0)$ and $\mu_\perp(\phi_0)$. Consequently, the thermal fluctuations in the order parameter will cause the effective masses to fluctuate as well. Since their distributions may be of some interest (see sect. 5.3), we consider briefly the corresponding probability densities for the effective masses,

$$P_\perp(\mu c^2) \equiv \int d^4\underline{\phi}\ P(\underline{\phi})\ \delta(\mu_\perp(\phi_0)c^2 - \mu c^2)\ , \tag{45}$$

and analogously for $P_{||}(\mu c^2)$, where $P(\underline{\phi}) = P_\phi(\phi_0)P_\chi(\phi_0; \chi_0)$ is the probability density for the order parameter $\underline{\phi}$. In order to gain an impression of these distributions, we show in fig. 9 the most probable effective masses as functions of the temperature.

The transverse effective mass $\mu_\perp$ increases steadily from its free value m_π as the temperature is raised, whereas the parallel effective mass $\mu_{||}$ drops by nearly fifty per cent before finally turning upwards. For temperatures above $T \approx 300$ MeV the two effective masses are practically degenerate and gently approach their asymptotic form $\mu c^2 \approx 1.59\ T$. We note that the effective masses always exceed the temperature, so it is never reasonable to ignore the effective masses. We also note that the transverse mass has practically no strength near the free pion mass, until the temperature is below T_0 (see fig. 13).

The parallel effective mass $\mu_{\|}$ exhibits a pronounced minimum at $T_\chi \approx 240$ MeV. It is in this region that the order parameter exhibits its most rapid evolution with T (see fig. 6) and the temperature T_χ at which the minimum in $\mu_{\|}$ occurs may be taken as the effective critical temperature of the model [29]. It is interesting to note that a recent study with a gauged linear sigma model [29] estimates this quantity as $T_\chi \approx 226$ MeV, a value in good accordance with the present results.

4.4 Sampling of the order parameter

The above analysis provides a convenient basis for sampling the order parameter in accordance with the statistical weight $W_T(\underline{\phi}, \underline{\psi})$ given in eq. (39), and we describe briefly how this can be accomplished in a manner that is both quick (*i.e.* the computational effort is small) and efficient (*i.e.* no effort is expended on rejection).

As noted already, the time derivative $\underline{\psi}$ is governed by a four-dimensional normal distribution which is isotropic and entirely decoupled from the other degrees of freedom (see eq. (42)). Thus it is elementary to sample this quantity.

The most complicated sampling concerns the magnitude ϕ_0, due to the intricate structure of its probability distribution, as discussed above. However, the numerical effort required is quite modest. The most efficient method requires a precalculation of the effective masses as functions of ϕ_0, for the particular T of interest. This is quickly done by proceeding as described in sect. 3.2. The χ_0-independent part of the effective potential, $V_T(\phi_0, 0)$, can then be obtained together with the corresponding entropy $S_T(\phi_0)$. In effect, the probability distribution for ϕ_0 can be pretabulated, $P_\phi(\phi_0)$ (see eq. (43)), and it is then a numerically trivial task to sample ϕ_0.

Once the magnitude ϕ_0 has been selected, it is straightforward to sample the disalignment angle χ_0, using either the exact form (44) or its Gaussian approximation. In order to orient $\underline{\phi}$ in the $\boldsymbol{\pi}$ subspace, there remains the task of selecting the remaining $O(3)$ spherical angles ϑ_0 and φ_0, upon which the order parameter is given by $\underline{\phi} = (\phi_0 \cos\chi_0,\ \phi_0 \sin\chi_0 \sin\vartheta_0 \cos\varphi_0,\ \phi_0 \sin\chi_0 \sin\vartheta_0 \sin\varphi_0,\ \phi_0 \sin\chi_0 \cos\vartheta_0)$.

5 The quasi-particles

We turn now to the discussion of the quasi-particle degrees of freedom associated with the spatial variations of the chiral field, $\delta\boldsymbol{\phi}(\boldsymbol{r})$. Once the magnitude of the order parameter, ϕ_0, has been chosen (see sect. 4.4), the quasi-particle degrees of freedom are fully characterized, via the effective masses $\mu_{\|}(\phi_0)$ and $\mu_\perp(\phi_0)$, and it is then possible to sample them appropriately.

5.1 Sampling

On the basis of the above developments, it is possible to devise a simple and efficient method for performing the statistical sampling of the chiral field, thus putting the initialization of dynamical simulations on a formally sound basis.

Since the different quasi-particle modes can be regarded as effectively decoupled, the sampling is best done by making an expansion into the elementary modes,

$$\delta\phi_{\|}(\boldsymbol{r},t) = \left(\frac{2}{\Omega}\right)^{\frac{1}{2}} {\sum_{\mathbf{k}}}' C^{\|}_{\mathbf{k}} \ \cos(\mathbf{k}\cdot\boldsymbol{r} - \omega^{\|}_k t - \eta^{\|}_{\mathbf{k}}) \ , \tag{46}$$

and similarly for the three transverse chiral components $\boldsymbol{\delta\phi}_{\perp}(\boldsymbol{r},t)$. Here the energy $\epsilon_k = \hbar\omega_k$ is determined by the Klein-Gordon dispersion relation, $\epsilon_k^2 = \hbar^2c^2k^2 + \mu^2c^4$ (with μ being the appropriate effective mass, $\mu_{\|}$ or $\mu_{\perp}$). The phase $\eta_{\mathbf{k}}$ is random in the interval $(0, 2\pi)$ and is thus trivial to sample. Furthermore, the real (and positive) amplitude $C_{\mathbf{k}}$ can be related to the number of quanta $n_{\mathbf{k}}$ by considering the energy carried by the mode,

$$E_{\mathbf{k}} = n_{\mathbf{k}}\epsilon_k = \frac{\epsilon_k^2}{\hbar^3c^3}C^2_{\mathbf{k}} \ \Rightarrow \ C_{\mathbf{k}} = \left[\hbar^3c^3\ \frac{n_{\mathbf{k}}}{\epsilon_k}\right]^{\frac{1}{2}} \ . \tag{47}$$

We have here omitted the zero-point energy [30], thereby eliminating the associated ultraviolet divergence. Although not quite correct, this approach is justified *a posteriori* by the apparent good quality of the resulting approximate treatment. (The dynamical tests discussed in sect. 6 are here very important, since the statistical samples would not remain stationary under time evolution if the treatment were substantially wrong.)

Thus the problem has been reduced to sampling the number of quanta $n_{\mathbf{k}}$. Since the probability for finding a particular number of quanta in the mode $\mathbf{k}$ is given by $P(n_{\mathbf{k}}) = (1 - \exp(-\epsilon_k/T))\exp(-n_{\mathbf{k}}\epsilon_k/T)$, it is elementary to sample the integer $n_{\mathbf{k}}$ appropriately.[5] We note that the thermal average of $n_{\mathbf{k}}$ is equal to the occupancy f_k employed in the calculation of the entropy, $\prec n_{\mathbf{k}} \succ = f_k$.

Once the amplitudes and phases have been selected, the expansion (46) readily yields the initial value of the field fluctuations, $\delta\boldsymbol{\phi}(\boldsymbol{r},0)$. The corresponding conjugate momentum, $\delta\boldsymbol{\psi} \equiv \hbar\partial_t\delta\boldsymbol{\phi}$, readily follows since (46) implies

$$\delta\psi_{\|}(\boldsymbol{r},t) = \left(\frac{2}{\Omega}\right)^{\frac{1}{2}} \sum_{\mathbf{k}} \epsilon^{\|}_k C^{\|}_{\mathbf{k}} \ \sin(\mathbf{k}\cdot\boldsymbol{r} - \omega^{\|}_k t - \eta^{\|}_{\mathbf{k}}) \ . \tag{48}$$

The entire state of the chiral field, $(\boldsymbol{\phi}(\boldsymbol{r}), \boldsymbol{\psi}(\boldsymbol{r}))$, has then been selected at the time $t = 0$. When the equations of motion are propagated by a leap-frog method, the field strength $\delta\boldsymbol{\phi}(\boldsymbol{r})$ is calculated at the times $t_n = n\Delta t$ while the momentum $\delta\boldsymbol{\psi}(\boldsymbol{r})$ is obtained at the intermediate times. The appropriate initial $\delta\boldsymbol{\psi}(\boldsymbol{r})$ can then easily be

[5]The corresponding algorithm for this task is very simple because $n_{\mathbf{k}}$ can be regarded as counting the number of successive times the sampling of a standard random number (*i.e.* uniform on $(0,1)$) yields a value below $\exp(-\epsilon_k/T)$.

obtained by evaluating the expansion (48) at $t = \Delta t/2$, after $C_{\mathbf{k}}$ and $\eta_{\mathbf{k}}$ have been selected.

Finally, since the sampling has been done in a system aligned with the order parameter $\underline{\boldsymbol{\phi}}$ (in which the mass tensor is diagonal), an $O(4)$ rotation of the sampled field configuration is required in order to express the state with respect to the chiral directions. This is readily accomplished on the basis of the angles $(\chi_0, \vartheta_0, \varphi_0)$ specifying the direction of $\underline{\boldsymbol{\phi}}$.

5.1.1 Occupation numbers

Since the quasi-particles represent bosonic modes, it is useful to know how large the occupancies can become. The thermal occupation numbers are given by $\prec n_{\mathbf{k}} \succ = f_k = 1/(\exp(\epsilon_k/T) - 1)$, and since $\mu_\perp < \mu_{||}$ in any given scenario the largest occupancies occur for the transverse modes, $f_k^\perp > f_k^{||}$. Moreover, for a given temperature T, f_k is largest when the momentum vanishes, $f_0 = 1/(\exp(\mu c^2/T) - 1)$, which then provides an upper bound on f_k (recall that $k > 0$ for the quasi-particles modes).

Considered as functions of T, the bounds $f_0^{||}$ and $f_0^\perp$ start out from zero, display maxima well above T_0, and then drop off towards a common constant value at high temperatures. The (common) limiting occupancy is $f_0 \approx 0.26$ since $\mu c^2 \approx 1.59T$ when $T \to \infty$. (This feature is a direct consequence of the repulsive self-interaction of the chiral field and is in marked contrast to the ever increasing occupancy characteristic of free bosons in a thermal bath.) The maximum values attained by $f_0^{||}$ and $f_0^\perp$ are about 0.38 and 0.48 and occur at approximately a temperature of 265 and 235 MeV, respectively. Since these values are well below unity, the system is never very degenerate.

Nevertheless, there is an important advantage to using Bose-Einstein rather than Boltzmann statistics for the field fluctuations, as we will now discuss. When classical statistics is used, the occupation probability is $n_k \approx T/\epsilon_k$, reflecting the equipartition theorem, and therefore the total energy density grows as the cube of the (required) cut-off on ϵ_k, a manifestation of the Rayleigh-Jeans divergence. Such a description would be entirely wrong in the present context and, moreover, it would be numerically ill-behaved. By contrast, the quantal occupation probability falls off exponentially and the density of quanta is finite. By adopting the Bose-Einstein treatment, we then get a much more realistic formal description of the statistical properties of the system and, in addition, the numerical treatment becomes straightforward. Of course, if a configuration sampled on the basis of the quantal statistics is propagated for a sufficient length of time, it will eventually exhibit classical features, since the equation of motion is entirely classical. It is therefore fortunate that our treatment is expected to be applied only to processes that are far faster than the time scales associated with the reversion to classical statistics. In particular, for the formation of disoriented chiral condensates in high-energy collisions the relevant time scales are of the order of a few fm/c, while our numerical studies exhibit no ultraviolet run-away for at least several tens of fm/c.

5.2 Correlation function

It is particularly interesting to calculate the correlation function of the chiral field since this quantity determines the spectral distribution of the emitted field quanta.

The density matrix associated with the quasi-particle degrees of freedom is a 4×4 tensor,

$$\boldsymbol{C}(r_{12},t_{12}) \equiv \prec \delta\boldsymbol{\phi}(\boldsymbol{r}_1,t_1)\ \delta\boldsymbol{\phi}(\boldsymbol{r}_2,t_2) \succ \ . \tag{49}$$

The average is over the ensemble of systems considered, in the present case a thermal ensemble held at the temperature T. Since an ensemble in equilibrium is invariant in time, the correlation function depends only on the time difference $t_{12}=t_1-t_2$. Analogously, the translational symmetry of the scenario implies that the spatial dependence is via the separation $\boldsymbol{r}_{12}=\boldsymbol{r}_1-\boldsymbol{r}_2$. Moreover, to the extent that there is invariance under spatial rotations, only the magnitude $r_{12}=|\boldsymbol{r}_{12}|$ enters. In principle, these spatial symmetries are broken when a finite box is considered but the effect is insignificant and can be disregarded in the present study.

Utilizing the expansion (46), it is elementary to show that the correlation tensor $\boldsymbol{C}$ is diagonal with the elements $C_{||}$ and $C_{\perp}$, where

$$C_{||}(r,t) = \frac{\hbar^3c^3}{\Omega}{\sum_{\mathbf{k}}}'\frac{1}{\epsilon_k}\frac{\cos(\mathbf{k}\cdot\boldsymbol{r}-\omega_k t)}{\mathrm{e}^{\beta\epsilon_k}-1} \asymp \frac{1}{2\pi^2}\frac{\hbar c}{r}\int_{\mu_{||}c^2}^{\infty} d\epsilon\ \frac{\sin kr}{\mathrm{e}^{\beta\epsilon}-1}\cos\omega_k t\ , \tag{50}$$

with $\epsilon_k^2=\hbar^2\omega_k^2=\hbar^2k^2c^2+\mu_{||}^2c^4$. An analogous expression holds for $C_{\perp}(\boldsymbol{r},t)$. Since $\hbar^3c^3f_k/\epsilon_k$ is equal to the thermal average $\prec C_{\mathbf{k}}^2\succ$, we recognize that the result (50) corresponds to the expression (146.10) given in ref. [21].

The usual correlation function is the trace of $\boldsymbol{C}$,

$$C \equiv \prec \delta\boldsymbol{\phi}(\boldsymbol{r}_1,t_1)\cdot\delta\boldsymbol{\phi}(\boldsymbol{r}_2,t_2)\succ = \mathrm{tr}\ \boldsymbol{C} = C_{||}(r_{12},t_{12})+3C_{\perp}(r_{12},t_{12})\ . \tag{51}$$

Its overall magnitude is set by its value at zero, which is simply the corresponding variance in the field strength, $C(0,0)=\prec\delta\phi^2\succ$. It is therefore convenient to divide C by this quantity and so define the reduced function $C_{12}\equiv C(r_{12},t_{12})/\prec\delta\phi^2\succ$. Since C_{12} is unity when $\boldsymbol{r}_1=\boldsymbol{r}_2$ and $t_1=t_2$, it expresses the space-time attenuation of the correlation between the field-strength fluctuations at different space-time points. In general, $C_{12}\sim(1/r_{12})\exp(-\mu c r_{12}/\hbar)$ in the limit of large separations, $r_{12}\to\infty$, so that $\hbar/\mu c$ provides a simple measure of the correlation length. In the special case when the effective mass vanishes, the reduced equal-time correlation function is given on analytical form, $C_{12}\asymp(3/\zeta)(\coth\zeta-1/\zeta)$, where $\zeta\equiv\pi T r_{12}/\hbar c$. In this extreme case, the correlation function falls off only as $\sim 1/r_{12}$.

Figure 10 shows the reduced correlation function C_{12} obtained at the particular temperature T_0. Its appearance depends on the magnitude of the order parameter, ϕ_0, through the effective masses. As ϕ_0 is increased from zero to its vacuum value $f_\pi=92$ MeV, the corresponding effective masses increase from zero to their free values and the correlation function falls off ever more rapidly. The correlation function thus exhibits a significant sensitivity to the order parameter. We note in particular that for the most probable value, $\phi_0\approx87$ MeV, the attenuation of C_{12} is considerably faster than for $\phi_0 = 0$ and its width has dropped by over a factor of two. It is therefore important to take proper account of the order parameter when calculating the correlation function.

Figure 11 shows how the reduced correlation function evolves with temperature when the most probable magnitude of the order parameter is employed. At high temperatures the effective masses grow nearly in proportion to T so then the correlation length tends to zero, as is borne out by the steady shrinking of C_{12}. For temperatures below critical, the field fluctuations are predominantly associated with the transverse modes, since those have the smallest effective mass, $\mu_\perp \ll \mu_{||}$, and the correlation length grows ever larger.

It is common to characterize the system by the "correlation length", defined as the first moment of the equal-time correlation function which diverges when $\mu \to 0$. For the present discussion, it is more convenient to characterize C_{12} by its full width at half maximum for equal times, Γ_{12}, since this quantity is always easy to extract, even when the mass vanishes. Figure 12 shows this measure of the correlation length as a function of temperature, using the most probable value of ϕ_0. For temperatures near and below $T \approx 200$ MeV the dominant fluctuations are perpendicular to the order parameter since the corresponding effective mass is relatively small. For higher temperatures the asymptotic regime is approached where the chiral symmetry is approximately restored and the fluctuations are similar in all four chiral directions.

It is sometimes of interest to also consider correlation functions involving $\delta\boldsymbol{\psi}$, the time derivative of the local field strength [11]. Those can be obtained in a similar manner.

5.3 Radiation spectra

The evolving chiral field may give rise to mesonic radiation, in analogy with the emission of photons by a time dependent electromagnetic field. The rate for production of a field quantum having energy E and momentum $\boldsymbol{p}$ is proportional to the square of the corresponding Fourier amplitude [31, 32, 33],

$$E\frac{dN_j}{d\boldsymbol{p}} \sim \left|\int d\boldsymbol{r} \int dt\ \delta\phi_j(\boldsymbol{r},t)\ \mathrm{e}^{-\frac{i}{\hbar}(\boldsymbol{p}\cdot\boldsymbol{r}-Et)}\right|^2 . \tag{52}$$

Here j denotes the particular $O(4)$ direction considered so that $j = 0$ gives rise to isoscalar σ-like mesons and $j > 0$ represent three components of the isovector pion-like mesons (with $j = 3$ corresponding to π_0, say).

A uniform system in equilibrium has both temporal and spatial invariance and the specific radiation rate, $\nu_j(\boldsymbol{p}, E)$ (*i.e.* the production per unit volume and per unit time), is then given by the Fourier transform of the correlation function [2],

$$\nu_j(\boldsymbol{p},E) \equiv \frac{1}{\Omega t_0} \prec E\frac{dN_j}{d\boldsymbol{p}} \succ \sim \int d\boldsymbol{r}\int dt\ C_j(r,t)\ \mathrm{e}^{\frac{i}{\hbar}(\boldsymbol{p}\cdot\boldsymbol{r}-Et)} \equiv \mathcal{C}_j(\boldsymbol{p},E) , \tag{53}$$

where Ω is the volume of the system and t_0 is the time interval considered. The Fourier transform of the correlation function is easy to obtain in the continuum limit,

$$\mathcal{C}_j(\boldsymbol{p},E) \asymp \hbar^3c^3\frac{\pi}{\mathrm{e}^{\beta E}-1}\ \delta(m^2c^4-\mu_j^2c^4) , \tag{54}$$

where we have assumed that the energy and momentum of the radiated mesons are related by $E^2 = p^2c^2 + m^2c^4$.

The above result holds for a specified value of the order parameter ϕ_0 which determines the effective mass μ_j. As we have discussed, the order parameter has in general a statistical distribution, $P(\phi_0)$, giving rise to corresponding distributions of the effective masses, $P_{||}(\mu)$ and $P_\perp(\mu)$ (see sect. 4.3.2). The resulting production rate can then be obtained by integrating over the appropriate thermal mass distribution. Thus, for example, the specific production rate for π_0 mesons is

$$\nu_{\pi^0}(\boldsymbol{p},E) \sim \int d\mu^2c^4 \; P_\perp(\mu^2c^4)\, \mathcal{C}_\perp(\boldsymbol{p},E) = \hbar^3c^3 \frac{\pi P_\perp(m_\pi^2c^4)}{e^{\beta E}-1}\;, \tag{55}$$

and the rates for the charged pions are similar.[6] This result is easy to interpret: The spectral distribution of the radiated mesons is of thermal Bose-Einstein form, with the temperature given by the value characterizing the source itself, and the overall normalization of the radiation rate is proportional to the probability that the space and time evolution of the field matches the particular dispersion relation for the type of meson considered.

As an illustration, fig. 13 displays the strength function $P_\perp(m_\pi^2c^4)$ obtained by evaluating eq. (45) for $\mu = m_\pi$ as a function of the source temperature. As the temperature is decreased towards zero, the centroid of the $\mu_\perp$ distribution moves down towards the free value m_π and at the same time its width keeps shrinking towards zero (see fig. 9). Through the supercritical regime the pion strength then grows approximately exponentially. Then a plateau is reached where the increase caused by the approach of the centroid to m_π is counterbalanced by the decrease due to the shrinkage. As a result, the strength is nearly constant from 90 to 30 MeV. Finally, after the centroid has practically reached m_π, the free strength exhibits a rapid rise as the $\mu_\perp$ distribution approaches a δ function. On the basis of this result, one would expect radiation of free pions to be unimportant until the temperature has dropped below T_0.

6 Dynamical tests

Once the initial state has been prepared, for example by means of the statistical sampling described above, the chiral field may be propagated in time by means of the equation of motion (9), which is straightforward to implement in either x or k representation.

It is possible to exploit the dynamical evolution to test the validity of our approximate statistical treatment. If the system is ergodic, as would be expected because of its non-linear interaction, a dynamical trajectory will explore the space of possible

[6]The rates considered here pertain to the idealized scenario of a macroscopically uniform system (possibly enclosed in a torus), and hence they differ from those describing the emission from a finite source into the surrounding vacuum. In particular, the familiar kinematic enhancement of the faster-moving ejectiles is absent.

field configurations in accordance with the appropriate microcanonical weight. Conversely, an ensemble of field configurations that has been sampled statistically should not exhibit any change under time evolution. These features provide a convenient means for checking our treatment and we give two illustrations below.[7]

6.1 Average field strength

Perhaps most vividly, we show in fig. 14 the early trajectories of the order parameter $\underline{\phi}$ for a sample of eight configurations, considering a box with $L = 8$ fm and either $T = 200$ MeV or $T = 240$ MeV. The dashed contours are those already given in fig. 8 indicating where the projected probability density has fallen to half its maximum value and the centroids are indicated as well (open dots). For each individual trajectory, the initial location is indicated by the solid dot and the attached solid curve shows the trajectory up to $t = 1$ fm/c. The fact that the initial points reflect the calculated statistical distribution provides an elementary test of the numerical sampling algorithms. Less trivial is the fact that the dynamical trajectories indeed appear to explore the region predicted by the approximate statistical distribution. When the propagation is continued for a longer time, up to 10-20 fm/c, each individual evolution exhibits a trajectory that gradually fills a localized region which appears to be well in accordance with the predicted equilibrium distribution, but such longer histories are not shown since they would clutter the display.

This correspondence can be made more quantitative by studying how the distribution of the order parameter evolves in the course of time. This analysis is illustrated in fig. 15. The approximate distribution $P_\phi(\phi_0)$ given in (43) is indicated by the solid curves for $T = 180$ and $T = 240$ MeV. Forty individual systems have then been prepared by sampling their field configurations as described above and they have subsequently been propagated by the equation of motion (9) up to the time $t = 10$ fm/c. In the course of the evolution, the value of ϕ_0 is extracted at regular intervals and binned into slots that are 5 MeV wide. In this manner the time-averaged distribution of ϕ_0 can be determined and the dashed curves display the result (which is not sensitive to an increase of either the maximum time or the sample size). The overall agreement with the initial distribution is very good. There is generally a slight shift outwards, amounting typically to 1-2 MeV, which suggests that our approximate thermal distributions may be centered at somewhat too low values of ϕ_0.

Propagations have been carried out up to $t = 100$ fm/c in order to get an impression of the long-term behavior. The results indicate a large degree of stability with respect to the domain explored by the order parameter in the course of time, but with a gradual evolution towards somewhat larger magnitudes. Such a trend is expected as a result of the diffusive population of high-frequency modes characteristic of classical dynamics. This mechanism effectively cools the system and hence softens the $O(4)$ restoring force. However, this gradual development happens on a time scale that is very long in the *DCC* context and it need therefore not concern us here.

[7]It is important to recognize that whereas the statistical properties have been obtained by assuming that the quasi-particle degrees of freedom are effectively decoupled, no such assumption is being made in the dynamics, since the trajectories are obtained by solving the full equation of motion (9).

6.2 Field fluctuations

Figure 16 displays the correlation function for the pion components, $C^{\pi}_{12}(s_{12})$, for a box with $L = 5$ fm prepared at $T = 240$ MeV. The short-dashed curves show the correlation function obtained on the basis of ten sampled configurations, and the long-dashed curves then indicate the corresponding result after those systems have been evolved up to the time $t = 10$ fm/c. The two curves that go up again have been obtained by aligning the relative separation $\boldsymbol{r}_{12}$ along one of the cartesian axes, while it is directed diagonally for the other two curves (the periodicity is then $\sqrt{3}L$ and so their eventual rise is only barely visible). For reference is shown the exact thermal correlation function for either the finite box considered (solid curves) or the continuum limit (dots). While this latter curve tends to zero for large separations (and in fact falls off monotonically), the correlation function for a finite box drops to a negative value, because its spatial average must vanish.

The correlation function remains remarkably invariant in the course of time. This suggests that our treatment, including the sampling procedure, in fact yields a good approximation to the correlated field fluctuations. As a quantitative measure, one may consider the full width at half maximum Γ_{12}. The continuum value is 1.33 fm, slightly larger than the thermal result for the finite box, 1.30. For the sample of ten initial configurations we find 1.256 and 1.271 for the cartesian and diagonal directions, respectively, which have evolved into 1.263 and 1.290 at $t = 10$ fm/c. So there is no significant change in the width of the correlation function over this time period.

6.3 Discussion

An additional perspective on the utility of the present approximate treatment may be obtained by considering the special case where H vanishes, even though that idealized scenario is not within the scope of intended applications. In this special case one expects a second-order phase transition to occur. Thus, in the limit of large volumes, $L \to \infty$, the order parameter should remain zero down to a critical temperature at which point it should start growing rapidly following a parabola-like trajectory down to its vacuum value v. When applying the developed approximate method with $H = 0$, we find that for high temperatures the free energy density has indeed its minimum at $\phi_0 = 0$ and the symmetric minimum grows ever more shallow as the temperature drops, as should be the case. Then, near $T \approx 175$ MeV, a very shallow secondary minimum appears at $\phi_0 \approx 50$ MeV, and it becomes the lowest one from about $T \approx 171$ MeV. As T decreases further that minimum gently approaches $\phi_0 = v$, again as one would expect.

However, the appearance of the secondary minimum causes an abrupt change in the location of the lowest minimum of the free energy, and so the order parameter exhibits a discontinuous change, as is characteristic of a first-order phase transition. Naturally, this feature might at first glance be a cause for concern. But, when trying to assess its significance, one should note that the energy differences responsible for producing the discontinuous behavior are only fractions of an MeV/fm^3. Consequently, if the calculated free energy density were adjusted by such small amounts, it would be possible to eliminate the shallow secondary minimum and thus convert the very weak first-order transition to a second-order transition.

The error in the employed approximation arises from the replacement of the state-dependent term δV by its thermal average $\prec \delta V \succ$. Although this is generally expected to be a fairly accurate approximation (the associated error being at the percentage level), it may easily lead to inaccuracies of the above small magnitude. Fortunately, while even such relatively small imperfections can thus produce a qualitative change very near the critical point for the idealized $O(4)$-symmetric model, they have little bearing on the situation of practical interest, since the finite value of H eliminates such critical sensitivity. Moreover, for finite systems of nuclear dimensions the associated distribution of the order parameter has a significant width and it is practically insensitive to such minor adjustments, even when H vanishes, as we already noted in connection with fig. 6. In particular, there is no discontinuity near the temperature where the location of the lowest minimum in the free energy changes abruptly.

7 Concluding remarks

The present work was motivated by the current interest in disoriented chiral condensates, particularly by the various dynamical simulations carried out with the linear σ model [8, 9, 11, 13, 14, 16]. Those calculations follow the non-equilibrium evolution of the cooling chiral field in order to ascertain the degree to which coherent domains develop. Since the dynamics is inherently unstable, with the low-momentum modes experiencing rapid amplification, one may expect a significant sensitivity of the results to the initial conditions, with a commensurate degree of difficulty regarding their interpretation. Consequently, caution is required when characterizing the ensemble of initial field configurations employed.

In order to provide a useful framework for this aspect of the problem, we have explored the statistical properties of the linear σ model in the form that is being used in the numerical simulations, *i.e.* propagation of classical fields in the presence of a finite symmetry-breaking term. In order to achieve a well-defined separation into order parameter and quasiparticles, we have confined the system to a torus and held it at a fixed temperature. Although this problem can be treated exactly [34], we have found it preferable to linearize the equations of motion by means of a Hartree-type approximation, since our view is towards practical calculations. The resulting treatment then becomes very simple and appears to be sufficiently accurate in the intended context. We also note that the treatment, though approximate, is thermodynamically consistent, since the partition function on which it is based has been obtained consistently within the adopted Hartree approximation scheme.

The problem separates into one concerning the spatial average of the field, the order parameter, and another dealing with the field fluctuations, referred to as the quasi-particle degrees of freedom. The latter are described approximately in terms of effective masses that depend on both the order parameter and the temperature, but are independent of the symmetry breaking H term; these were presented in fig. 1.

The partition function then takes on a corresponding separable form and, as a consequence, it is possible to develop a simple method for performing a statistical sampling of the thermal equilibrium field configurations, including their time derivatives, at any temperature (even if subcritical). It has the combined advantages of being less cumbersome than exact stochastic methods, such as Metropolis sampling, and having a clear physical basis that brings out the interplay of the various quantities entering. The method is expected to be directly useful as practical means for initializing the dynamical simulations of the chiral field of the type carried out recently by several groups [8, 9, 11, 13, 14, 16], thus making it easier to interpret the numerical results. The developed sampling method presents a significant improvement over the previously employed method which simply samples the field strength independently at each lattice point and thus yields a very unrealistic correlation function.[8]

Moreover, our specific illustrations provide useful insight into the equilibrium properties. In particular, it appears to be unrealistic to start the order parameter off with a value equal to zero. Indeed, for temperatures up to more than 200 MeV the most probable order parameter is closer to its vacuum value f_π than to zero. The relationship between temperature and order parameter was summarized in fig. 6 and a more global impression of the distribution of the the order parameter (including its degree of misalignment) can be gained from the contour plots in fig. 8.

Since the order parameter is thus very unlikely to vanish, the effective quasi-particle masses remain finite. Consequently, the statistical equilibrium distribution is well behaved at all temperatures and the change from the "restored" phase to the normal one is fairly gradual. However, the finite size generally reduces the effective masses, thereby bringing the system somewhat closer to criticality (which should enhance the DCC phenomenon).

Of course, the statistical properties are of most practical interest at the relatively high energy densities characteristic of the initial stage of the high-energy collision. Once the chiral field has been initialized accordingly, any instabilities and associated amplifications will be automatically included in the dynamical propagation and the system can generally be expected to quickly move out of equilibrium. The equilibrium results can then provide a meaningful reference against which to analyze the deviation from equilibrium at any stage in the dynamical relaxation process.

Additionally, we illustrated briefly the equilibrium form of the correlation function which is an object of primary interest. Indeed, it is the correlation length that properly expresses the "domain size" governing the conjectured anomalous pion radiation. Essentially, what one would expect to see at the end is a stretched version of the initial correlation function since the long wave lengths are the most unstable and so will contribute in an ever larger proportion. This underscores the importance of starting out with chiral fields that have physically reasonable correlation properties.

[8]One might attempt to remedy this shortcoming by propagating this initial white noise for a while in order to get closer to equilibrium before starting the actual simulation. However, such an approach is somewhat dubious because of the tendency of the field to relax towards the appropriate classical equilibrium (since it is propagated by a classical field equation of motion) which is neither desirable (since the quasiparticle degrees of freedom are bosonic in nature) nor attainable (because of the Rayleigh-Jeans divergence).

To illustrate the use of the correlation function, we derived the rate at which real pion mesons are created by the field, and subsequently we calculated the dependence of the free pion strength on the temperature of the system.

Finally, we sought to assess the accuracy of our approach by subjecting sampled field configurations to the exact time evolution. This convenient means of testing suggested that the approximate treatment is of sufficient accuracy to be of practical utility. We therefore anticipate that it may find use in simulation studies, such as those exploring disoriented chiral condensates in high-energy collisions.

The author is pleased to acknowledge helpful discussions with many colleagues, including P. Bedaque, L.P. Csernai, S. Gavin, J.I. Kapusta, Y. Kluger, V. Koch, L. McLerran, E. Mottola, R.D. Pisarski, K. Rajagopal, R. Vogt, and X.N. Wang.

References

[1] K. Rajagopal, in *Quark-Gluon Plasma 2*, ed. R. Hwa, World Scientific (1995)

[2] S. Gavin, Nucl. Phys. A590 (1995) 163c

[3] A.A. Anselm, Phys. Lett. B217 (1989) 169;
A.A. Anselm and M.G. Ryskin, Phys. Lett. B266 (1991) 482

[4] J.-P. Blaizot and A. Krzywicki, Phys. Rev. D46 (1992) 246

[5] K. Rajagopal and F. Wilczek, Nucl. Phys. B399 (1993) 395

[6] C.M.G. Lattes, Y. Fujimoto, and S. Hasegawa, Phys. Rep. 65 (1980) 151;
J.R. Ren *et al.*, Phys. Rev. D38 (1988) 1417;
L.T. Baradzei *et al.*, Nucl. Phys. B370 (1992) 365

[7] K.L. Kowalski and C.C. Taylor, Report CWRUTH-92-6 (1992);
J.D. Bjorken, K.L. Kowalski, and C.C. Taylor, Report SLAC-PUB-6109 (1993)

[8] K. Rajagopal and F. Wilczek, Nucl. Phys. B404 (1993) 577

[9] S. Gavin, A. Gocksch, and R.D. Pisarski, Phys. Rev. Lett. 72 (1994) 2143

[10] S. Gavin and B. Müller, Phys. Lett. B329 (1994) 486

[11] F. Cooper, Y. Kluger, E. Mottola, and J.P. Paz, Phys. Rev. D51 (1995) 2377;
Y. Kluger, F. Cooper, E. Mottola, J.P. Paz, and A. Kovner, Nucl. Phys. A590 (1995) 581c

[12] J.-P. Blaizot and A. Krzywicki, Phys. Rev. D50 (1994) 442

[13] Z. Huang and X.-N. Wang, Phys. Rev. D49 (1994) 4335

[14] M. Asakawa, Z. Huang, and X.-N. Wang, Phys. Rev. Lett. 74 (1995) 3126

[15] D. Boyanovsky, H.J. de Vega, and R. Holman, Phys. Rev. D51 (1995) 734

[16] L.P. Csernai and I.N. Mishustin, Phys. Rev. Lett. 74 (1995) 5005

[17] S. Mrówczyński and B. Müller, Phys. Lett. 363B (1995) 1

[18] J. Randrup, Phys. Rev. Lett. 77 (1996) 1226

[19] The literature is abundant with studies of models with $O(N)$ symmetry and the following limited selection of references may help guide readers interested in that subject: S. Coleman and E. Weinberg, Phys. Rev. D7 (1973) 1888; L. Dolan and R. Jackiw, Phys. Rev. D9 (1974) 3320; G. Baym and G. Grinstein, Phys. Rev. D15 (1977) 2897; W.A. Bardeen and M. Moshe, Phys. Rev. D34 (1986) 1229; R. Allés and R. Tarrach, Phys. Rev. D33 (1986) 1718; W. Buchmüller, T. Helbig, and D. Walliser, Nucl. Phys. B407 (1993) 387. A general discussion of second-order phase-transitions can be found in ref. [21].

[20] N. Tetradis and C. Wetterlich, Nucl. Phys. B398 (1993) 659

[21] L.D. Landau and E.M. Lifshitz, *Statistical Physics*, Pergamon, New York (1980)

[22] M. Gell-Mann and M. Levy, Nuovo Cimento 16 (1960) 705

[23] M. Aguilar-Benitez *et al.*, Phys. Rev. D50 (1994) 1173

[24] G. Baym and G. Grinstein, Phys. Rev. D15 (1977) 2897

[25] E. Medeiros de Lima and J. Randrup, Nucl. Phys. A529 (1991) 115

[26] M. Toda, R. Kubo, and N. Saitô, *Statistical Physics I*, Springer, New York (1992)

[27] W.A. Bardeen and M. Moshe, Phys. Rev. D34 (1986) 1229

[28] Y. Kluger, private communication (1996)

[29] R.D. Pisarski, Phys. Rev. D52 (1995) R3773

[30] J.I. Kapusta, *Finite-temperature field theory*, Cambridge University Press, New York (1989)

[31] D. Horn and R. Silver, Ann. Phys. 66 (1971) 509

[32] M. Gyulassy, S.K. Kauffmann, and L.W. Wilson, Phys. Rev. C20 (1979) 2267

[33] R.D. Amado, F. Cannata, J.P. Dedonder, M.P. Locher, and Bin Shao, Phys. Rev. Lett. 72 (1994) 970

[34] J. Bernstein and S. Dodelson, Phys. Rev. Lett. 66 (1991) 683

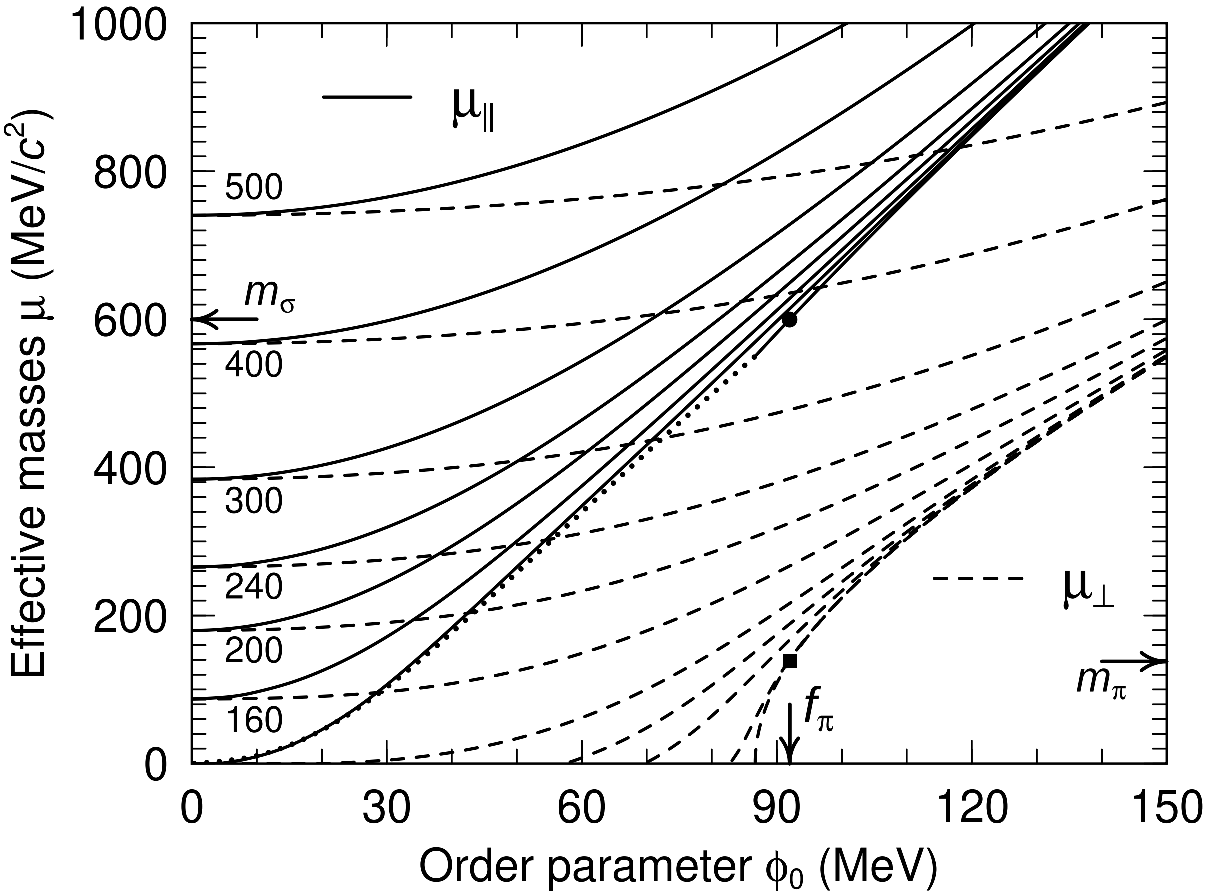

Figure 1: Effective masses.

The effective masses $\mu_{||}$ (solid) and $\mu_\perp$ (dashed), as functions of the magnitude of the order parameter, ϕ_0, for a range of temperatures: T = 0, 40, 80, 100, 122.63 (=T_0), 160, 200, 240, 300, 400, 500 MeV, calculated in the thermodynamic limit where the box size is large, $L \to \infty$. For a temperature above T_0, the two effective-mass curves start out at $\phi_0 = 0$ with degenerate values, whereas below T_0 they only exist if ϕ_0 is sufficiently large. The corresponding starting points for $\mu_{||}$ are connected by the dotted curve and, since $\mu_{||}$ is then nearly independent of T, only the curve for $T = 0$ has been shown. The vertical arrow points to the vacuum value of the order parameter, $\phi_{\rm vac} = f_\pi = 92$ MeV, and the free mass values $\mu_{||} = m_\sigma = 600$ MeV/c^2 and $\mu_\perp = m_\pi = 138$ MeV/c^2 are indicated by the horizontal arrows. The locations of the corresponding points in the diagram are shown by the two solid symbols.

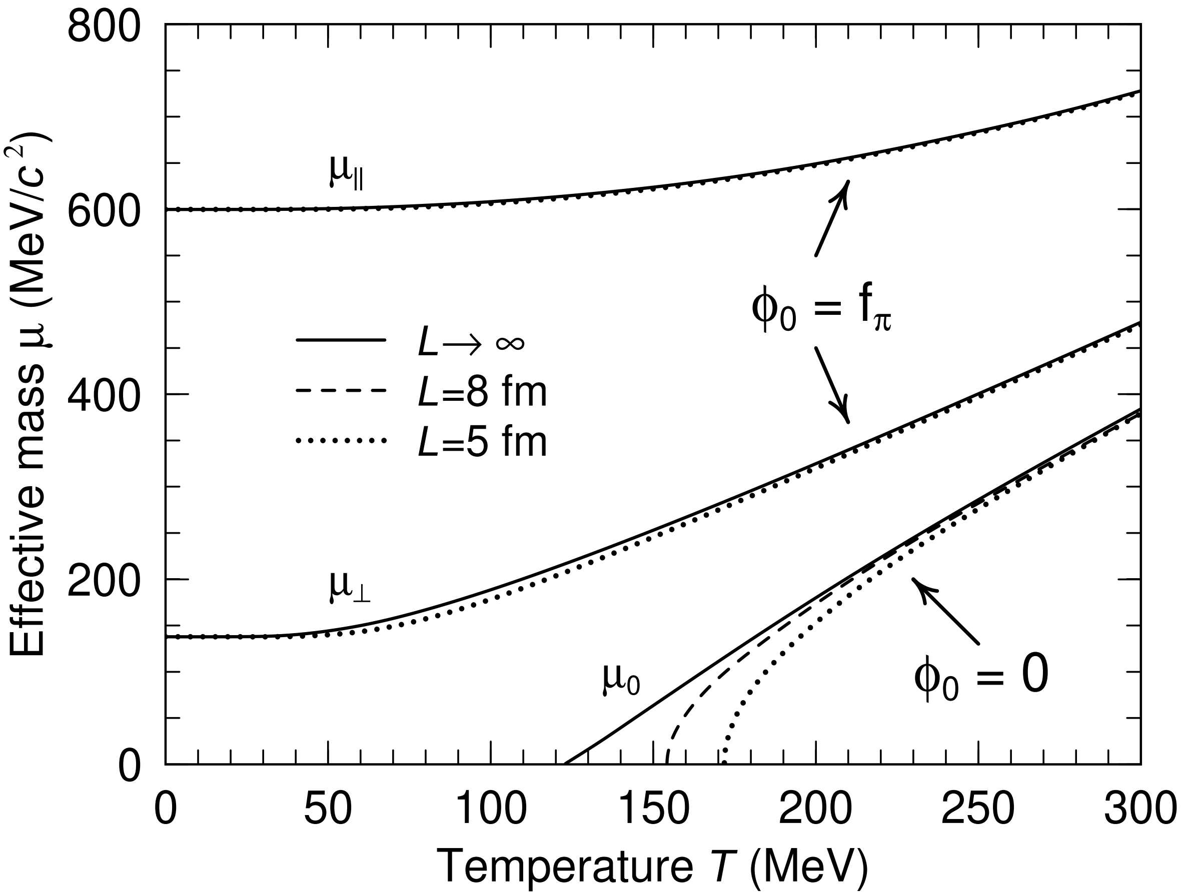

Figure 2: Effect of finite size on the effective masses.
The effective masses are shown as functions of the temperature for either $\phi_0 = 0$, when the $O(4)$ symmetry is restored, or for $\phi_0 = f_\pi$, the physical vacuum value. Three different scenarios have been considered: either the thermodynamic limit of large volume in which the quasi-particle spectrum is continuos (solid curve), corresponding to the scenario of fig. 1, or a finite cubic box with side length $L = 8$ fm (dashed) or $L = 5$ fm (dotted), where the quasi-particle modes are quantized.

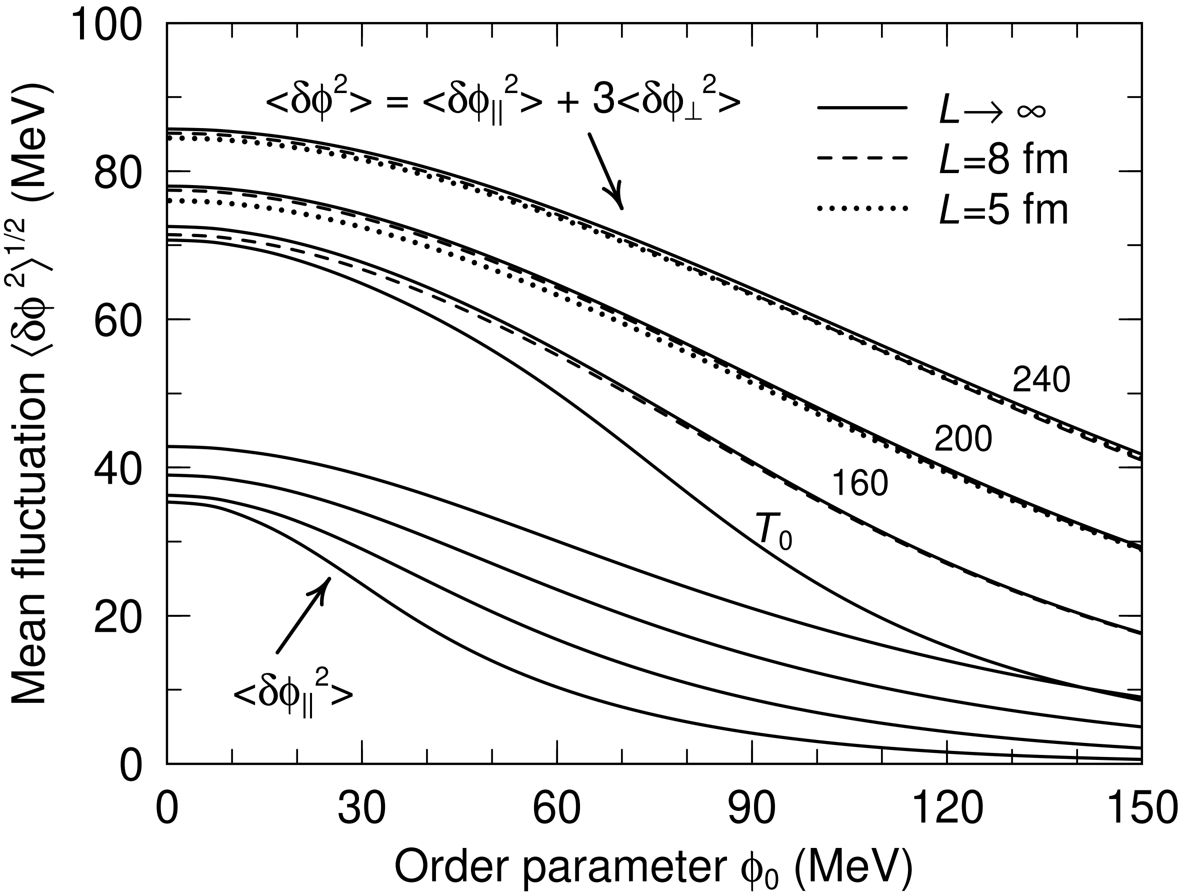

Figure 3: Fluctuations.

The typical magnitude of the spatial fluctuations in the field strength, $\prec \delta\phi^2 \succ^{1/2}$, as a function of the magnitude of the order parameter, ϕ_0, for specified temperatures T: 122.63 (=T_0), 160, 200, 240 MeV. The system is enclosed in a cubic box of side length $L \to \infty$ (solid curves), $L = 8$ fm (dashed), or $L = 5$ fm (dotted). The lower four curves display the fluctuations along the chiral direction of the order parameter $\underline{\phi}$, while the upper curves represent the total fluctuation.

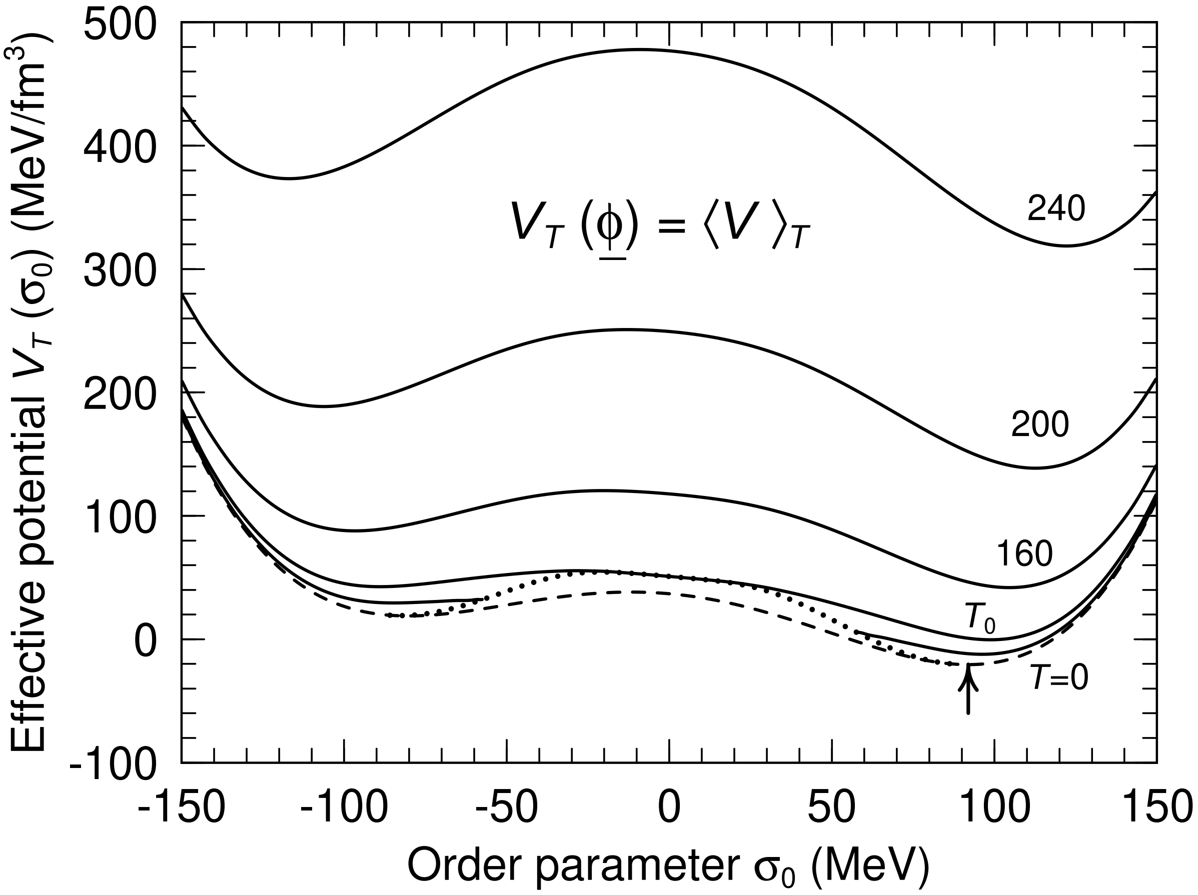

Figure 4: Effective potential.

The effective potential energy density V_T along the σ axis for a range of temperatures. The solid curves show the results for a number of temperatures: 100, 122.63 (=T_0), 160, 200, 240 MeV. For $T < T_0$ the effective potential curve starts at a certain minimum value of ϕ_0 between 0 and v, These starting points are connected by the dotted curve, while the dashed curve shows the bare potential V_0 obtained when fluctuations are neglected. The arrows point to the minima of V_T; for $H > 0$ there is only a single minimum (located at $\sigma_0 = f_\pi$), while for $H = 0$ the degenerate ground-state minima form the surface of the 4-sphere determined by $\phi = v$. The value of the effective potential corresponding to other orientations of the order parameter can be easily obtained by noting that the directional dependence of V_T is given by $-H\phi_0 \cos\chi_0/\hbar^3c^3$.

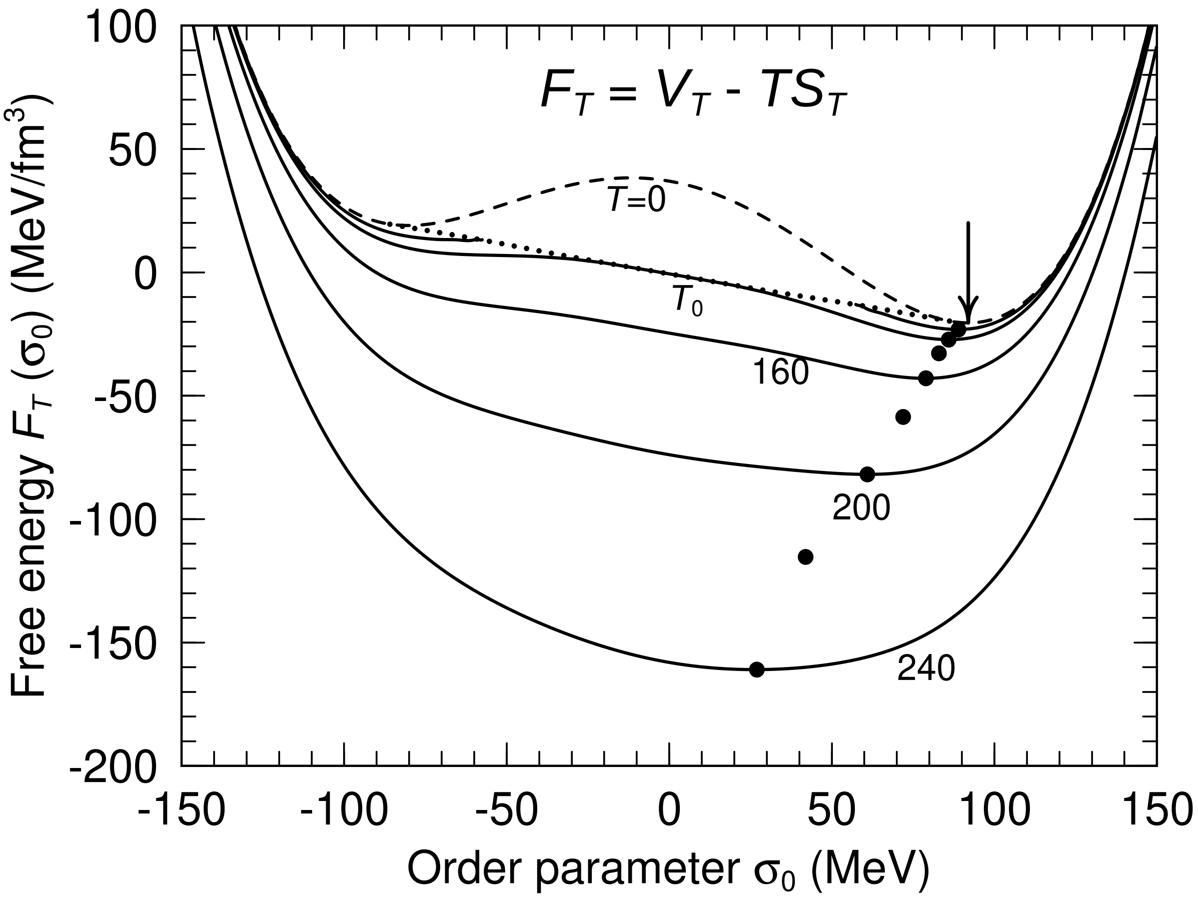

Figure 5: Free energy.
The free energy density $F_T(\underline{\phi})$ along the σ axis for a range of temperatures. The solid curves show the results for a number of temperatures. For $T < T_0$ the curve starts at a certain minimum value of the magnitude ϕ_0 and these starting points are connected by the dotted curve, while the dashed curve shows the result obtained when the temperature is neglected. The arrow points to the minima of $F_{T=0}$ and for the finite temperatures the location of the minima are indicated by the solid dots.

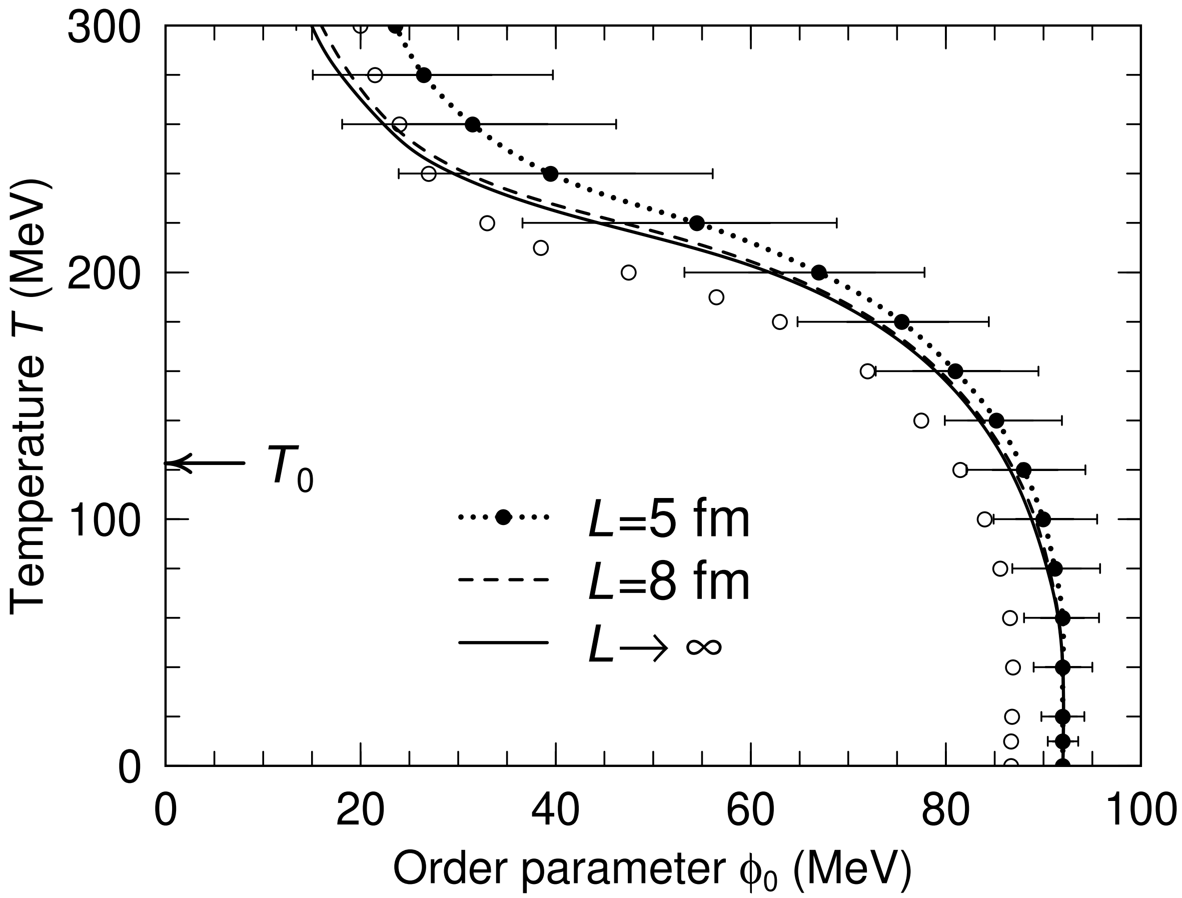

Figure 6: Temperature dependence of the order parameter.
The most probable value of ϕ_0, the magnitude of the order parameter, in the standard model where $H > 0$. In the limit of a very large box, $L \to \infty$ (solid curve) ϕ_0 is constrained to the value for which the free energy density has its minimum (see fig. 5*b*). The bars show the full width at half maximum of the thermal distribution of ϕ_0 in the system with $L = 5$ fm; those for $L = 8$ fm are about half that size (see fig. 7). The open dots show the centroids for $H = 0$ for the box with $L = 5$ fm.

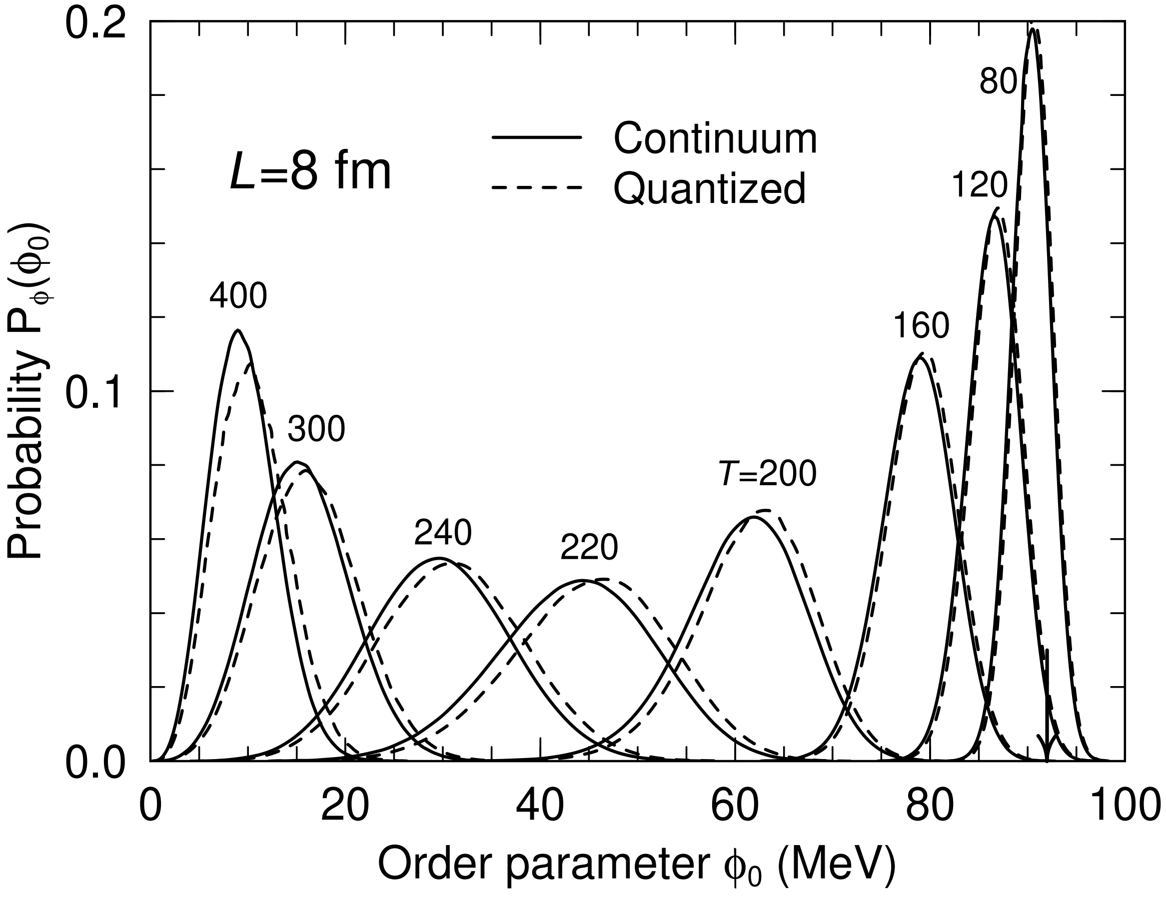

Figure 7: Distribution of the magnitude of the order parameter.
For a cubic box of side length $L = 8$ fm is shown the probability density for the magnitude of the order parameter, $P(\phi_0)$, for a range of specified temperatures T (indicated), obtained either by scaling the continuum result (solid curves) or by quantizing the quasi-particle modes (dashed curves).

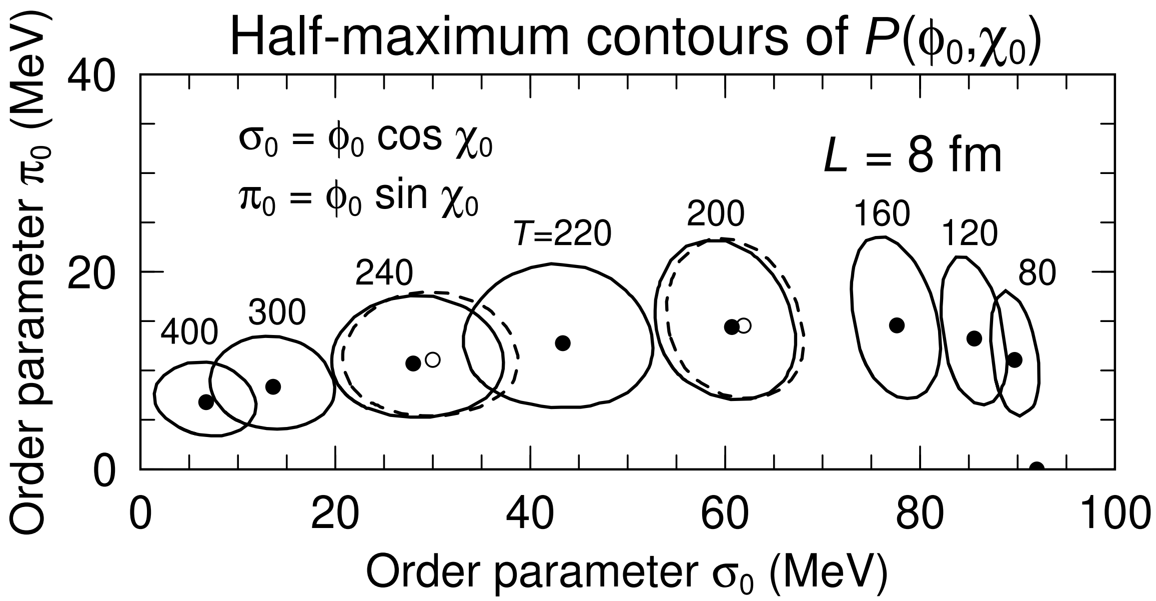

Figure 8: The joint distribution $P(\phi_0, \chi_0)$.
The projection of the probability density $P(\underline{\phi})$ onto the variables ϕ_0 (the magnitude of the order parameter) and χ_0 (the disalignment angle) is displayed as a function of $\sigma_0 = \phi_0 \cos\chi_0$ and $\pi_0 = \phi_0 \sin\chi_0$, for a cubic box of side length $L = 8$ fm. For each temperature T, the solid dot indicates the location of the maximum of $P(\phi_0, \chi_0)$ and the solid curve traces out the half-maximum contour, obtained by scaling the continuum results. For the temperatures 200 and 240 meV is indicated the corresponding result of quantizing the quasi-particle modes (dashed contours and open centroid dots).

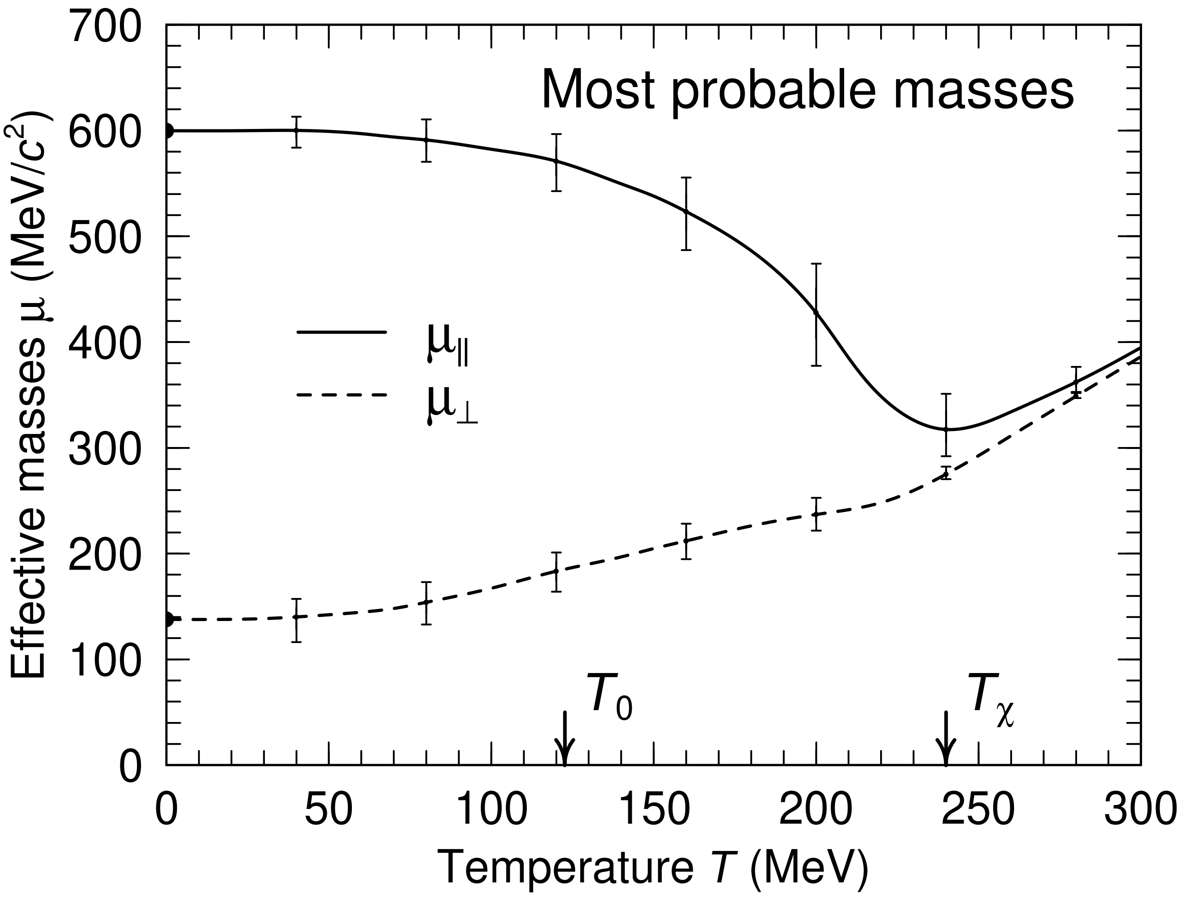

Figure 9: Most probable effective masses.
The most probable effective masses $\mu_\parallel$ (solid) and $\mu_\perp$ (dashed) are shown as functions of the temperature T, with the error bars indicating the full width at half maximum of the distribution resulting for a box with a side length of $L = 8$ fm. The results obtained by scaling the continuum results are indistinguishable from those of the corresponding quantized treatment.

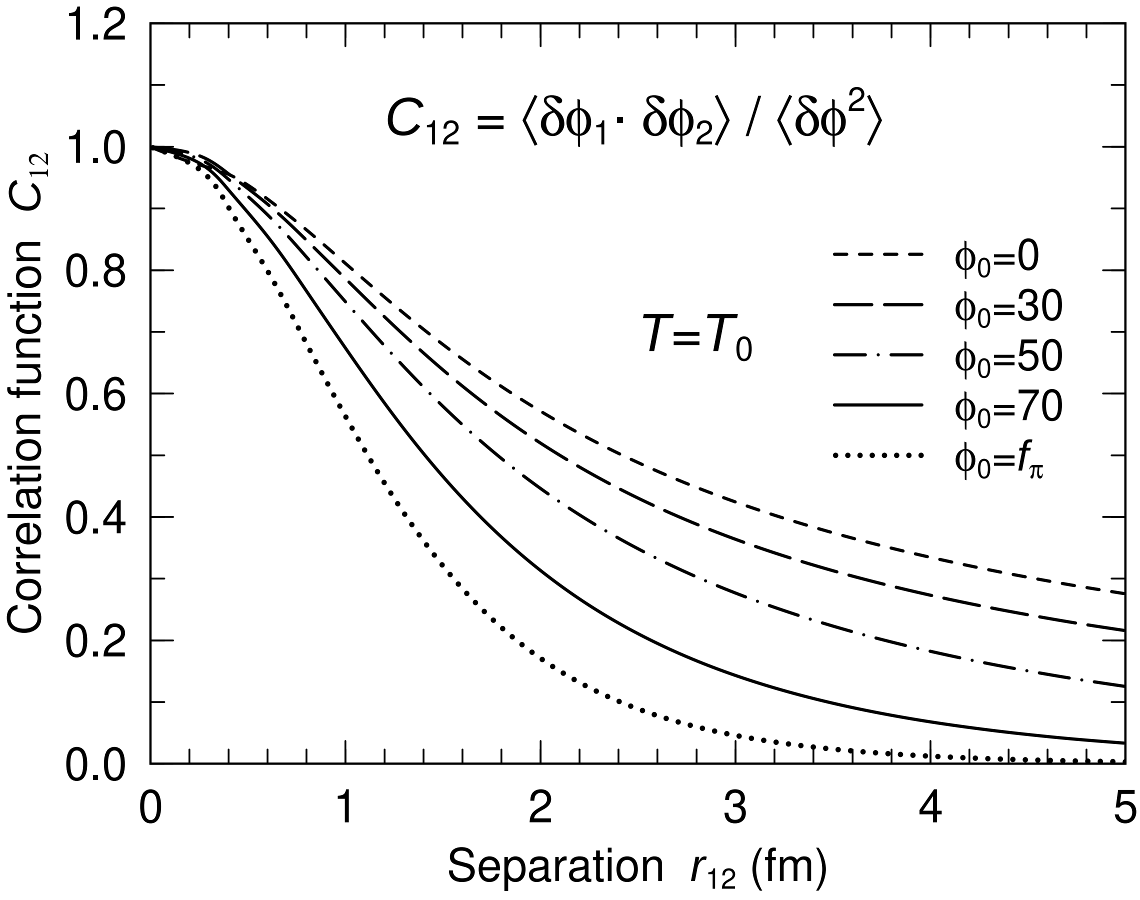

Figure 10: Correlation function at T_0.
The reduced correlation function $C_{12} = \prec \delta\boldsymbol{\phi}(\boldsymbol{r}_1) \cdot \delta\boldsymbol{\phi}(\boldsymbol{r}_2) \succ / \prec \delta\phi^2 \succ$ calculated at the special temperature T_0 (for which the effective masses vanish when $\phi_0 = 0$), for various magnitudes of the order parameter, ranging from $\phi_0 = 0$ to the vacuum value, $\phi_{\rm vac} = f_\pi = 92$ MeV. The most probable value of ϕ_0 at T_0 is ≈ 87 MeV.

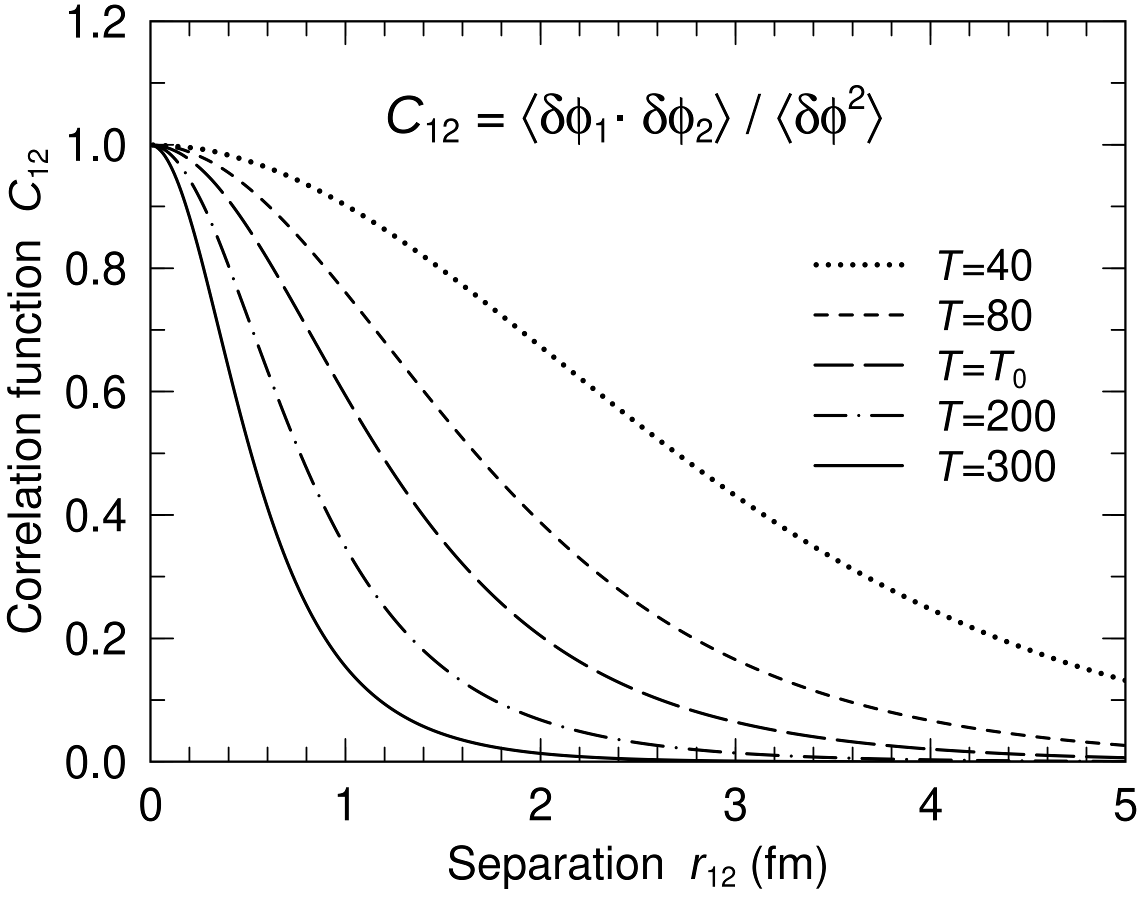

Figure 11: Temperature dependence of correlation function.
The reduced correlation function C_{12} for a range of temperatures T, employing for each one the most probable value of ϕ_0, the magnitude of the order parameter.

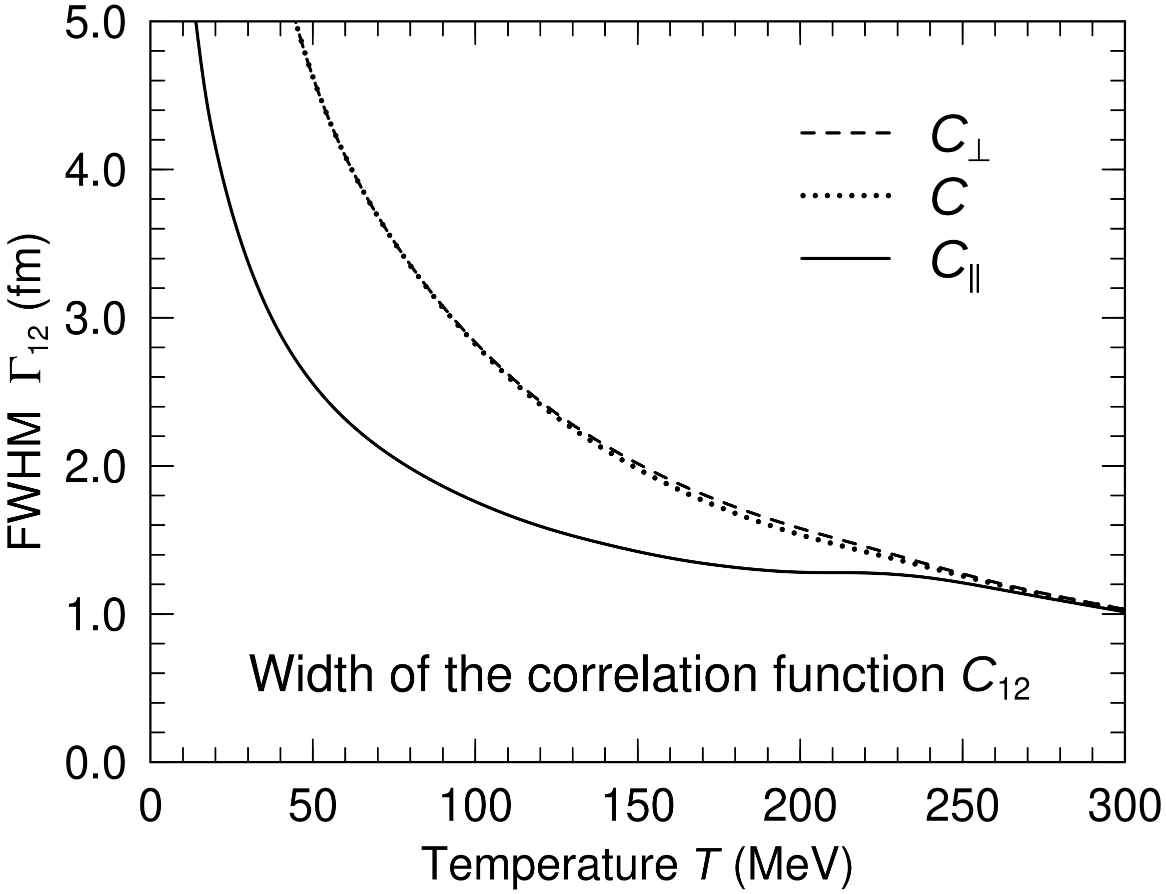

Figure 12: Correlation length.
The correlation length Γ_{12} (the full width of C_{12} at half maximum) as a function of temperature, employing the most probable value of ϕ_0 for each T.

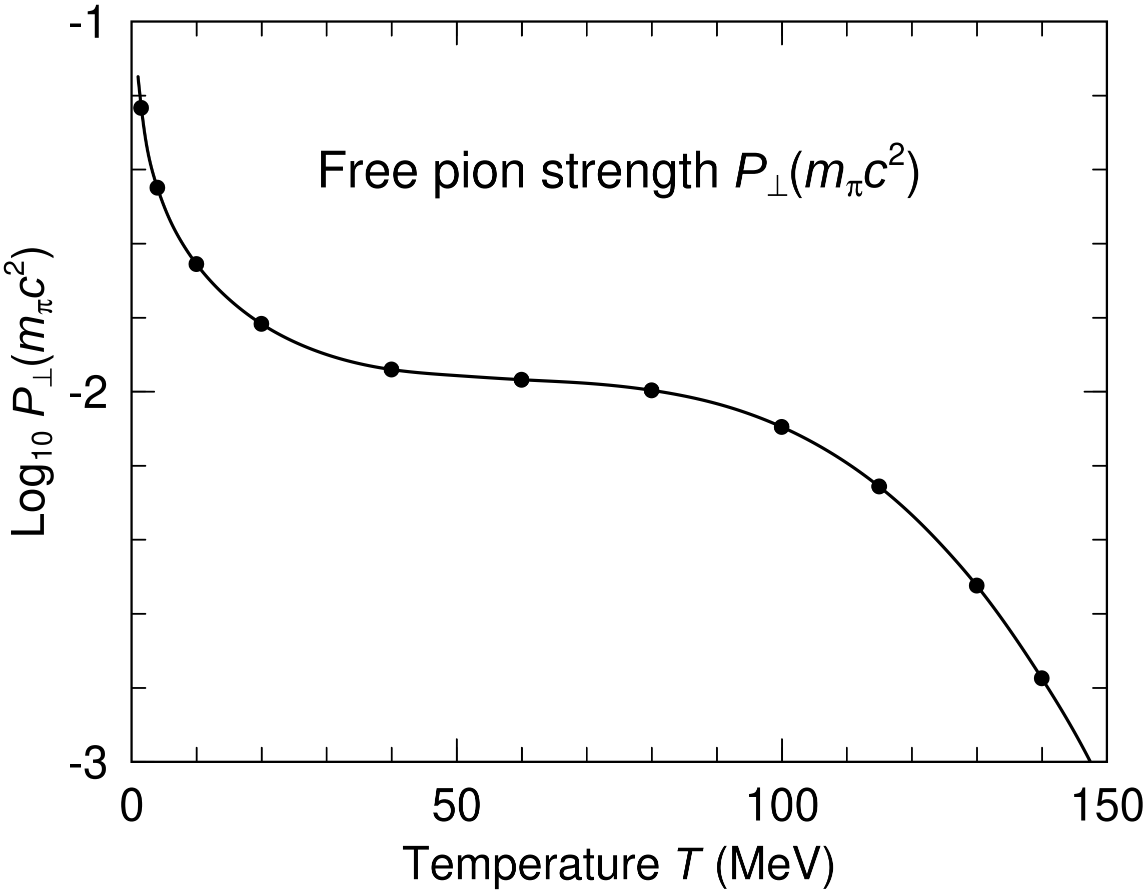

Figure 13: Pion production rate.
The strength function $P_\perp(m_\pi c^2)$ determining the overall rate at which π^0 mesons are being produced (see eq. (55)) in a source in thermal equilibrium, as a function of its temperature T. This result is obtained by performing a Fourier transform of the quasi-particle correlation function associated with a given order parameter ϕ_0 and subsequently averaging over its distribution, $P_0(\phi_0)$. The overall normalization is arbitrary.

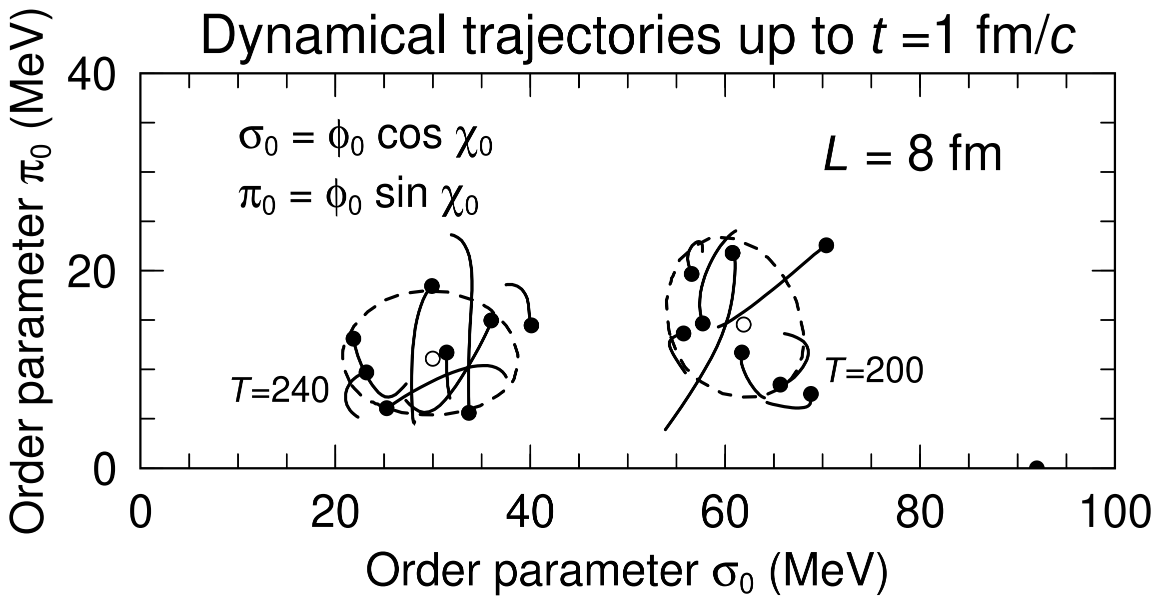

Figure 14: Early dynamics of the order parameter.
The early trajectories of the order parameter is shown for a sample of eight configurations, considering a box with $L = 8$ fm with a temperature of either 200 or 240 MeV. The display is similar to that in fig. 8 and the half-density contours (dashed) as well as the centroids (open dots) are those already given there. For each individual trajectory, the initial location is indicated by the solid dot and the attached solid curve traces out the dynamical path up to the time $t = 1$ fm/c.

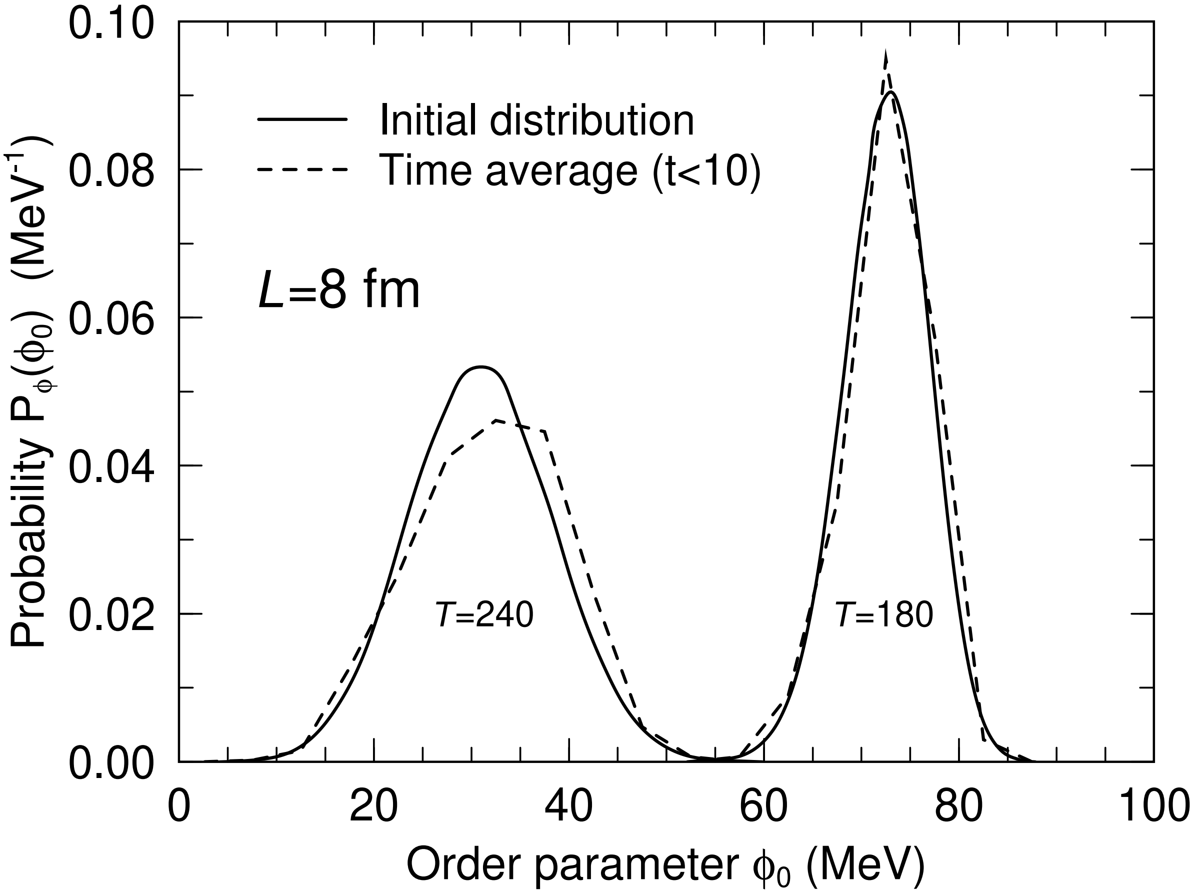

Figure 15: Time-averaged distribution of the order parameter.
This figure illustrates the influence of the time evolution on the distribution of the magnitude of the order parameter, ϕ_0, for a bow with $L = 8$ fm and for the temperatures of 180 and 240 MeV. The solid curves show the initial distribution of ϕ_0, as given by approximate statistical distribution $P_\phi(\phi_0)$ (see eq. (43)). A sample of 40 systems are then followed up to the time $t = 10$ fm/c and the order parameter is binned at regular time intervals throughout the evolution, leading to the dashed curves.

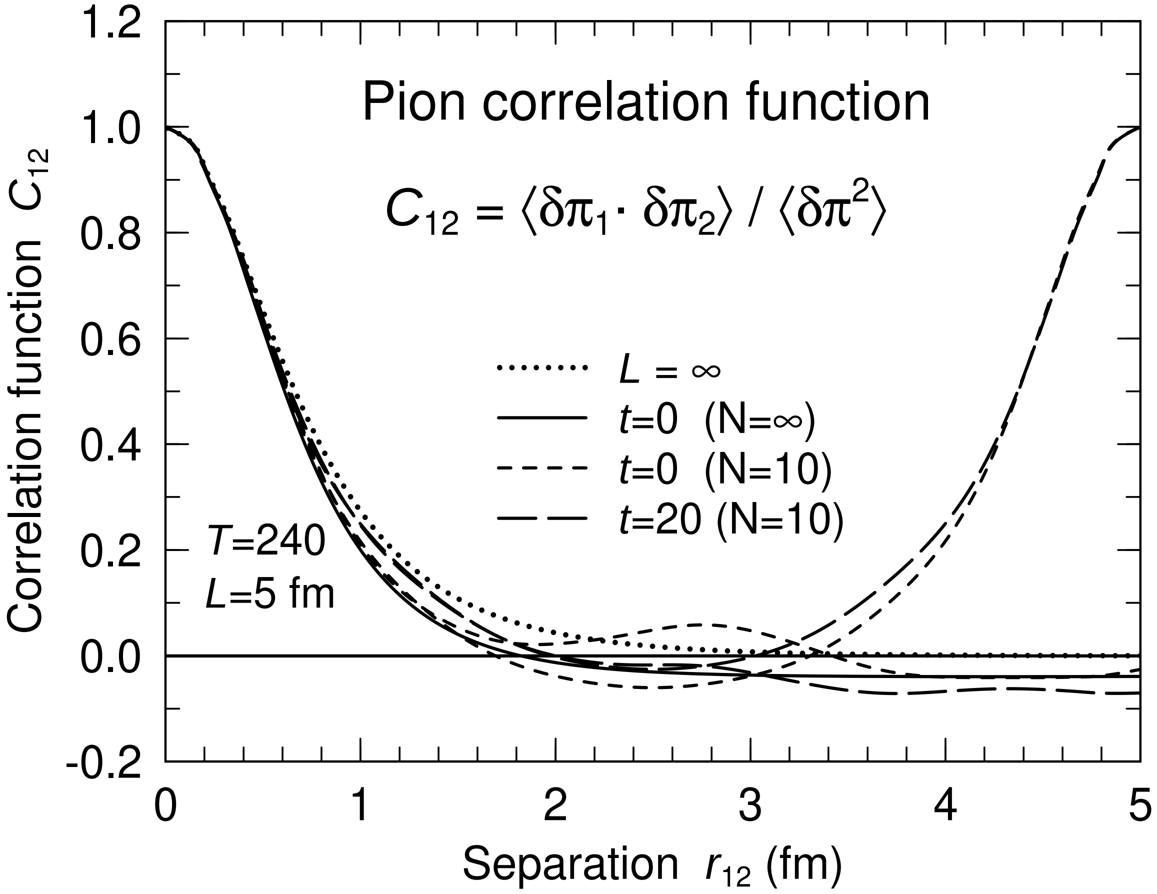

Figure 16: Time evolution of the correlation function.
The pion correlation function $C^{\pi}_{12}(s_{12})$ at the temperature $T = 240$ MeV. The dotted curve is the continuum limit ($L \to \infty$) and the solid curve is the corresponding thermal result for a quantized finit box with a side length of $L = 5$ fm. The correlation function for a sample of ten initial configurations are shown by the short-dashed curves, and the long-dashed curves show the corresponding result after they have been propagated self-consistently up to the time $t = 10$ fm/c. The dashed curves have been obtained in two different ways: The curves that go up again result from aligning the separation $\boldsymbol{r}_{12}$ along one of the cartesian directions, while the other two are obtained for separations directed along a diagonal. The aligned curves have a periodicity equal to L, whereas the periodicity of the diagonal curves is $\sqrt{3}$ times larger.